Probabilistic Assessment of Flood Hazard due to Levee Breaches Using Fragility Functions

Probabilistic Assessment of Flood Hazard due to Levee Breaches Using Fragility Functions

M. D'Oria[1], A. Maranzoni[1], and M. Mazzoleni[2]

[1]Department of Engineering and Architecture, University of Parma, Parco Area delle Scienze 181/A, 43124 Parma, Italy.

[2]Centre of Natural Hazards and Disaster Science, Uppsala University, Villavägen 16, 75236 Uppsala, Sweden.

Corresponding author: A. Maranzoni (andrea.maranzoni@unipr.it)

Key Points:

- A probabilistic method is presented to assess inundation hazard due to piping-induced levee breaches in flood-prone areas.
- Scenarios are defined in terms of breach locations and times, and their probabilities are estimated using fragility functions.
- The method is applied to a case study in northern Italy to show its capabilities in probabilistic flood hazard mapping.

Abstract

Flood hazard maps are useful tools for land-planning and flood-risk management in order to increase the safety of flood-prone areas that can be inundated in the event of levee failure. However, flood hazard assessment is affected by various uncertainties, both aleatory and epistemic. The flood hazard analysis should hence take into account the main sources of uncertainty and quantify the confidence of the results for a given design flood event. To this end, this paper presents a probabilistic method for flood hazard mapping which considers uncertainty due to breach location and failure time. A reliability analysis of the discretized levee system, performed using the concept of fragility function, enables the pre-selection of a set of levee sections more susceptible to failure. The probabilities of the breach scenarios (characterized by different breach locations and times) are then calculated using the probability multiplication rule, neglecting multiple breaches. The method is applied to a 96 km levee-protected reach in the central portion of the Po River (northern Italy) and to an adjacent 1900 km^2 flood-prone area on the right-hand side of the river, with a focus on the piping breach mechanism. The numerical simulations are performed through a combined 1D-2D hydrodynamic model using widespread free software. The results show that the method is effective for probabilistic inundation and flood hazard mapping. In addition, it has the advantage of requiring a smaller computational effort in comparison with the methods based on a classic Monte Carlo procedure.

1 Introduction

Hydrological and meteorological hazards have increased worldwide in the last decades, and floods, together with storms, are currently the most recurrent natural disasters, causing the most fatalities, and major social impact and economic damage (CRED, 2018a). An estimated 2.0 billion people were affected by floods in the period 1998-2017, and the recorded economic losses amounted to US$ 656 billion (CRED, 2018b). In view of this, the recent international efforts to mitigate the impact of floods appear fully justified. Among these, the European Floods Directive 2007/60/EC (European Commission, 2007; de Moel et al., 2009) and the US National Flood Insurance Program (FEMA, 2016) require flood hazard assessment and mapping for flood safety and risk management purposes. Moreover, several national and international research projects have been funded to investigate extreme flood processes and study effective methodologies for flood risk assessment and management (e.g., IMPACT, 2005; FLOODsite, 2009). Several reports and guidance to flood risk reduction published in recent years (e.g., USACE 1997; DEFRA, 2006; USACE 2017) confirm the attention of national governments to this issue in order to achieve a more flood-resilient society (Merz et al., 2014; Surminski & Thieken, 2017).

Flood risk assessment essentially consists in the estimate of the likelihood and severity of the adverse consequences of a flood event. It rationally supports a risk-based decision-making process aimed at developing effective risk communication and flood management policy, as well as at orienting judicious land-use planning and economic resources allocation (e.g., Sayers et al., 2002; Hall et al., 2003; Apel et al., 2004; Dawson et al., 2005; Gouldby et al., 2008; Sayers et al., 2010; Harvey et al., 2014; Wagenaar et al., 2016). The flood hazard assessment, i.e. the quantification of the frequency and severity of a flooding event, is a fundamental phase of the overall flood risk analysis (USACE, 2017).

The flood hazard analysis can be advantageously applied also to flood-prone areas located close to river reaches and protected by levee systems, because of the residual risk due to potential levee breaches. Moreover, these areas often attract socio-economic activities, and are hence characterized by high exposure and vulnerability. Among the possible mechanisms causing a levee to breach (see, e.g., Wolff, 1997), under-seepage and through-seepage through the levee foundation or the levee core (with consequent retrogressive internal erosion and piping) are particularly worrying. Indeed, these phenomena can unexpectedly occur for ordinary flood events too, even in the recession stage, and can be triggered by hidden soil discontinuities, such as burrows (Orlandini et al., 2015; Palladino et al., 2019). Statistics related to several levee failures have also shown that piping is the most frequent breaching mechanism after overtopping (e.g., Vorogushyn et al., 2009; Vorogushyn et al., 2010; Mazzoleni et al., 2015).

The accurate prediction of the flooding extent and the assessment of the related hazard are essential for a comprehensive and effective management of the residual flood risk, despite the inherent uncertainties affecting the parameters involved in the analysis. Due to the absence of standardized methodology to accomplish these tasks, several methods have been proposed in literature (see the review by Teng et al., 2017) which can be classified as probabilistic or deterministic depending on whether the scenarios considered in the analysis include an estimate of their frequency of occurrence (Bates et al., 2004; Di Baldassarre et al., 2010; Beven et al., 2015). The deterministic approach is based on design scenarios suggested by empirical considerations or historical information, characterized by predefined breach locations and times, and by a single optimum parameter set calibrated against observed data, when available (e.g., Aureli & Mignosa, 2004; Aureli et al., 2006a; Aureli et al., 2006b). However, because of the uncertainty in breach location and failure time, such approach requires considering a number of different scenarios in order to provide meaningful results for flood risk management decisions. Moreover, a sensitivity analysis on the model parameters (e.g., roughness coefficient, breach size, etc.) is advisable in this case in order to take into account their inherent uncertainty and assess the effect of their variability on the results (e.g., Hesselink et al., 2003). On the other hand, in the probabilistic approach, the scenarios considered are coupled with their probability of occurrence, thereby providing a measure of the associated aleatory and epistemic uncertainties (Aronica et al., 2002; Romanowicz & Beven, 2003; Hall & Solomatine, 2008; Merwade et al., 2008; Merz and Thieken, 2009; Di Baldassarre et al., 2010; Dottori et al., 2013). Accordingly, the flooding extents and hazard levels predicted can be accompanied by an estimate of the related uncertainty, expressed in terms of probability. Several sources of uncertainty affect flood hazard and flood risk assessment (Apel et al., 2004; Bales & Wagner, 2009; Teng et al., 2017; Winter et al., 2018), including the model boundary conditions (e.g., Pappenberger et al., 2006; Domeneghetti et al., 2013), the topographic data and the hydraulic parameters involved in the flood propagation modeling (e.g., Pappenberger et al., 2005; Jung & Merwade, 2015), as well as the levee failure location and the breach parameters (Wahl, 2004). In any case, both the deterministic and probabilistic approaches require that key hydraulic variables describing the dynamics of the inundation (typically flood depth, velocity, and arrival time) are evaluated through suitable hydrodynamic models, which are usually validated against historical flood data (e.g., Hesselink et al., 2003; Di Baldassarre et al., 2009a; Horritt et al., 2010; Masoero et al., 2013; Vacondio et al., 2016).

105 The probabilistic approach has recently gained great attention, and a large number of
106 probabilistic methods have been proposed in literature to assess residual risk (e.g., Apel et al.,
107 2004; Apel et al., 2006; Smemoe et al., 2007; Merwade et al., 2008; Vorogushyn et al., 2010;
108 Aronica et al., 2012; Domeneghetti et al., 2013). In particular, in recent years, several studies
109 have taken into account uncertainty in breach position and geometry for probabilistic flood
110 hazard mapping in flood-prone areas potentially subject to inundation as a result of a levee
111 failure (e.g., Van Der Most & Wehrung 2005; Apel et al., 2009, Vorogushyn et al., 2009,
112 2010, 2011; Mazzoleni et al., 2015, 2017, Tyagunov et al., 2018). In addition, semi-
113 probabilistic methods, which provide weight-averaged probabilistic flood hazard maps
114 without explicit quantification of the associated uncertainty, are proposed by Di Baldassarre
115 et al. (2009b), Viero et al. (2013), and Mazzoleni et al. (2014). The aforementioned
116 probabilistic methodologies are typically based on Monte Carlo simulations that require a
117 significant computational effort and can be prohibitive for wide river domains and complex
118 topographies.

119 In order to overcome this limitation, this paper presents a new probabilistic method
120 for the assessment of the flood hazard due to inundations subsequent to piping-induced levee
121 breaches. The method identifies potential levee failure scenarios (defined in terms of breach
122 locations and times) by using the probabilistic information on the levee reliability provided
123 by the concept of fragility function, thereby avoiding computationally expensive Monte Carlo
124 simulations. The fragility functions provide the probability of levee failure (for a specific
125 breach mechanism) at selected locations as a function of the hydraulic load. By using this
126 information, each breach scenario can be coupled with its probability, which represents how
127 likely the scenario is for a design flood event of fixed return period. Such scenario
128 probabilities are calculated by applying the probability multiplication rule for dependent
129 events to the failure probabilities derived from the fragility functions of the successive
130 selected levee sections, and neglecting multiple breaches. Furthermore, it is assumed that the
131 levee breach can occur not only at the peak water level (as commonly hypothesized), but at
132 previous times too, thus configuring breach scenarios potentially more dangerous for the
133 adjacent flood-prone area. Breach location and failure time are actually among the aspects
134 which impact more heavily on the dynamics of the subsequent inundation and, consequently,
135 on the flood hazard assessment in the floodable area. Finally, probabilistic inundation and
136 hazard maps are generated for the flood-prone area by performing a spatial probability
137 analysis of the maximum water depths and flow velocities obtained from the numerical
138 simulation of each inundation scenario, and of the predicted maximum value of a suitable
139 flood hazard index.

140 In order to show its effectiveness in probabilistic flood hazard mapping, the method is
141 applied to a 96 km levee-protected reach in the central portion of the Po River (northern Italy)
142 and an approximately 1900 km^2 flood-prone area on the right-hand side of the river. The
143 flood simulations are performed through a combined 1D-2D hydrodynamic model using the
144 free software HEC-RAS (Brunner, 2016a). The classification proposed by DEFRA (2006) is
145 adopted for the flood hazard assessment.

2 Method

The probabilistic method proposed in this paper is based on a chain of three main modules (Figure 1).

The first module consists in a probabilistic levee breach model aimed at describing the reliability (against a given failure mechanism, piping in this study) of a discretized levee system, by pre-selecting potential sections susceptible to failure, and identifying potential breach scenarios characterized by different failure locations and times, with associated probabilities. To this end, the concept of fragility function and the probabilistic multiplication rule for dependent events are employed. The levee breach scenarios identified are then utilized in the second module to simulate the dynamics of the inundations caused by the corresponding breaching events. A combined 1D-2D hydrodynamic model is used to simultaneously simulate the river flood routing between the main levees through a 1D model and, in the event of a levee failure, the subsequent inundation of the flood-prone area through a 2D model. Finally, the results of the numerical simulations are processed in the third module through a spatial probability analysis model to calculate probabilistic flood inundation and hazard maps.

The main assumptions of the method are:
1) The analysis is performed for a design flood event of given return period.
2) Only piping is considered among the various levee breach mechanisms.
3) The topographic data, the spatial distribution of the roughness coefficient (in both the river channel and the flood-prone area), the upstream and downstream river boundary conditions are treated in a deterministic way, i.e. like model inputs free of uncertainty. Only levee porosity is considered as a stochastic variable in deriving the fragility functions for piping.
4) The geometric characteristics of the breaches (length and shape) are treated deterministically and are fixed a priori.
5) The levee failure can only occur during the rising stage of the flood wave, when the hydraulic load increases with time. Moreover, it is assumed that the load is applied separately on the successive pre-selected levee sections, in a sequential way from upstream to downstream, according to the propagation of the flood in the river.
6) Multiple breach scenarios are ignored, i.e. it is excluded that the levee may breach in different locations during the same flood event.

The three modules of the method are described in detail in the following subsections.

Here Figure 1

2.1 Probabilistic levee breach model

The levee breach module (see Figure 1) is based on a reliability model which allows fragility curves for piping at each section of the discretized levee system to be obtained. In general, the levee performance function depends on various geometrical and geotechnical variables which in principle are all uncertain. Among these, only the levee porosity is considered as a stochastic variable in this paper, since its value is often highly uncertain due

to the high soil heterogeneity encountered in practical applications. Accordingly, levee porosity variability must be described through a probability density function (PDF). The conditional failure probabilities for given water levels derived from the fragility functions at selected levee sections are converted into breach scenario probabilities (for a given design flood event of assigned return period) by applying the probability multiplication rule for dependent events, as explained in detail below. The probability of each breach scenario (defined in terms of breach location and time) is then applied to the corresponding flooding, which is modeled by the hydrodynamic module.

2.1.1 Levee reliability model

The fragility function is a well-established mathematical tool commonly used in structural engineering and risk assessment in order to provide a description of the resistance capability of a protection structure subject to an external load (Schultz et al., 2010). This concept is also applied to earthen levees in flood hazard analysis by considering different failure mechanisms (e.g., Wolff, 1997; USACE, 1999; Hall et al., 2003; Dawson et al., 2005; Apel et al., 2006; Vorogushyn et al., 2009; Mazzoleni et al., 2015; Camici et al., 2017).

In general, the reliability of a defense system is described by a limit state function G defined as the difference between the limit resistance R of the protection structure and the external load L (e.g., FLOODsite, 2007; Vorogushyn et al., 2009; Mazzoleni et al., 2015; Marijnissen et al., 2019):

$$G = R - L. \tag{1}$$

Accordingly, the failure occurs when $G < 0$. When dealing with the reliability of levees to piping, Eq. (1) can be rewritten as

$$G = j_c - j, \tag{2}$$

in which j_c is the critical hydraulic head gradient triggering piping (which is dependent on the geotechnical properties of the levee), and j is the slope of the hydraulic grade line of the seepage flow (and associated piping) through the levee. According to Covelli (2006) and Mazzoleni et al. (2015), based on the equation proposed by Khilar et al. (1985), j_c can be expressed as a function of the levee total porosity n only as

$$j_c = C\frac{1-n}{n} \quad (0 \le n \le 1), \tag{3}$$

C being a positive dimensionless constant equal to 0.237. Hence, Eq. (2) becomes

$$G = C\frac{1-n}{n} - \frac{\eta}{L}, \tag{4}$$

in which η represents the water level in the river with reference to the landside levee toe elevation, and L is the horizontal projected length of an idealized seepage path. Figure 2 shows the definition of these variables and sketches the two main categories of levee configurations which can be encountered in piping failure analysis: in Figure 2a the landside levee toe is higher than the riverside one, whereas the opposite occurs in Figure 2b. As shown in Figure 2, L is considered as a decreasing function of η (which depends on the inner-side

slope of the bank) and in a simplified way can be assumed to approximate the water seepage length in the case of through-seepage in the levee core. This situation is potentially more dangerous than the case of under-seepage, in which L coincides with the length of the levee foundation.

Here Figure 2

If the porosity is treated as a stochastic variable in Eq. (4), the reliability function $G(n; \eta)$ becomes a stochastic variable too, describing the levee system reliability for a given hydraulic load η in a probabilistic way. According to the rule of transformation of stochastic variables (e.g., Henderson & Plaschko, 2006), the probability density function of $G(n)$ (the dependence on the parameter η is omitted for clarity) is

$$f_G = f_{n(G)} \left| \frac{dn}{dG} \right|, \tag{5}$$

in which f_n is the probability density function of the variable n and $n(G)$ denotes the inverse of the function defined in Eq. (4). It is worth noting that, according to Eq. (4), $G(n)$ is a strictly monotonic decreasing function, and thus it is invertible. Its inverse function is

$$n(G) = \frac{C}{G + \frac{\eta}{L} + C}, \tag{6}$$

from which

$$\left| \frac{dn}{dG} \right| = \frac{C}{\left(G + \frac{\eta}{L} + C \right)^2}. \tag{7}$$

If a simple probability density function $f_n(n)$ is assumed for n, an analytical expression for $f_G(G)$ can be derived from Eq. (5) using Eqs. (6) and (7), and the cumulative probability function $P_G(G)$ can then be obtained by integration. Since the failure limit state of the protection system is attained for $G = 0$, P_G calculated at $G = 0$ provides the probability $P_G(G \leq 0 \mid \eta)$ of levee failure due to piping as a function of the hydraulic load η (i.e. conditioned to the hydraulic load), which represents the fragility function $P_f(\eta)$ for piping at a selected levee section.

A triangular probability density distribution is assumed for levee porosity n in the case study presented in the next section (see Appendix A for details), with n ranging from $n_{\min} = 0.25$ to $n_{\max} = 0.55$. This range is suitable for compacted heterogeneous soils which typically constitute earthen embankments and foundations. Mode n_0 is set at 0.45, so that the probability density distribution of n is asymmetric toward the highest values of the porosity range, which are typical of fine sediments. The mean and median values of n are approximately 0.417 and 0.423, respectively. As an example, Figure 3 shows the fragility curve obtained for $n_0 = 0.45$ at one of the cross-sections of the levee system analyzed in the

case study, along with the curves that can be obtained for different values of n_0 (n_0 = 0.30, 0.35, 0.40, and 0.50). In Figure 3, the fragility functions are fictitiously extended (with dashed lines) over the levee crest supposing the levee crown to artificially extend upwards, in order to draw the curve up to P_f = 1. This example shows that the probability of failure for piping can be significantly less than unity even for water levels near the levee crown, if the levee is well designed and sufficiently thick. The sensitivity analysis on n_0 shows that the greater n_0, the greater the failure probability P_f at a fixed hydraulic load η. This means that, for the selected probability density function f_n, lower modal values n_0 induce a better performance of the levee against failure due to piping, ensuring that breach probability remains lower as the flood water level increases.

The previous levee reliability analysis can in theory be easily adapted to any arbitrary probability density distribution function f_n and can be extended to other types of levee failure mechanism. A numerical method based on a Monte Carlo procedure can be adopted when the analytical derivation of the fragility curves is not possible or excessively difficult (e.g., Vorogushyn et al., 2009; Mazzoleni et al., 2015).

Here Figure 3

2.1.2 Assessment of the breach scenario probabilities

The levee breach module is based on the idea that fragility functions can be utilized to identify a set of potential breach scenarios, defined in terms of breach location and failure time. To this end, a preliminary 1D flood routing simulation is performed by assuming that no levee breaches occur along the river reach, in order to predict the peak water levels at the cross-sections used to discretize the river and to "pre-select" a set of locations (denoted by LS_i, i = 1, …, N in Figure 4) where the discretized levee system is more susceptible to failure. The total number N of pre-selected levee sections depends on the severity of the loading flood event (i.e. its return period), for fixed geometrical and geotechnical characteristics of the levee. The probabilities corresponding to each scenario can then be assessed using the probability multiplication rule for dependent events, and must be regarded as probabilities conditional on a loading flood event of given return period.

As mentioned in the previous subsection, fragility functions provide a measure of the vulnerability of a levee section (to a specific breach mechanism) as a function of the water stage, by considering the resistance of each levee section as independent of the others. However, the concept of fragility function is based on the assumption that external loading is applied statically, whereas a levee is subject to a dynamic loading, with water levels changing over time during a flood event. Reaching a certain peak water level at a selected river cross-section depends on several factors, mainly including the severity of the input hydrological event, the intensity of the attenuation effect during the propagation of the flood wave in the river, and the occurrence of breaches at adjacent locations (especially upstream), which can significantly reduce water levels, depending on the breach length and the failure time.

Levee breaching at a selected cross-section does not necessarily occur at the peak flood level ($\eta = \eta_{max}$) when the hydraulic load is maximum, but it can happen at lower water

stages, even belonging to the rising limb of the flood wave, albeit with lower probability. Indeed, these intermediate flood states can induce significant seepage in the levee core and foundations, especially for long duration floods, thus realistically triggering piping. In these cases, conservative (from an engineering point of view) and potentially more dangerous failure scenarios originate, in which greater water volumes can be expected to flow out of the breach (and, consequently, higher flood hazard levels occur in the flood-prone area) compared to the case in which the levee breaches at the peak water level. To take into account the uncertainty affecting breach time, the physically relevant portion of the fragility curves (for $\eta \leq \eta_{max}$) can be discretized through a suitable number of points, as shown in Figure 4. Hence, an ensemble of loading conditions $\eta_{i,k}$ potentially inducing levee breaching can be defined for each pre-selected section; the first subscript index $i = 1, \ldots, N$ refers to pre-selected section LS_i, while the second subscript index $k = 1, \ldots, N_i$ to the selected discrete loading stages (in increasing order), N_i being the total number of loading stages (corresponding to different potential failure times) considered for LS_i. Accordingly, η_{i,N_i} denotes the peak water level η_{max} predicted at section LS_i. As an example, in the case study presented in the next section, the partition of the fragility curves into discrete pieces is based on 5% probability intervals, and hence the number of loading water stages considered (including the peak one) is int[$P_{f(LS_i)}(\eta_{i,N_i})/0.05$] + 1, which varies from a levee section to another depending on the peak water level predicted (and hence the maximum failure probability), and on the features and shape of the corresponding fragility functions. This discretization criterion allows the fragility curves to be described with sufficient detail. Increasing discrete loading levels implies that a greater number of potential breach scenarios with less probability of occurrence will have to be considered at a given levee section.

Here it is assumed that a levee can only fail during the rising phase of the flood wave, when it is subject to an increasing load. The occurrence of a breach at section LS_i for loading $\eta_{i,k}$ obviously excludes the possibility that another breach event occurs later at the same location for higher water levels. This means that, at a selected levee section, breach events induced by different water stages are mutually exclusive, and a failure at LS_i for loading level $\eta_{i,k}$ can only occur if the levee has not failed there previously at lower water levels $\eta_{i,1}, \ldots, \eta_{i,k-1}$. In light of this, the probability that a levee section breaches for a given discrete load (and no breaches occurred earlier at lower levels) can be derived from the fragility curves by assuming that the failure probability provided by them for $\eta_{i,k}$ includes the probability concerning $\eta_{i,k-1}$ (and lower discrete water levels). The fragility function can then be interpreted as a cumulative failure probability function, and can also be used in the case of unsteady loading events with increasing load. Accordingly, the difference $P_{f(LS_i)}(\eta_{i,k}) - P_{f(LS_i)}(\eta_{i,k-1})$ represents the probability of failure of levee section LS_i when water level $\eta_{i,k}$ is reached, excluding the probability of previous failures at $\eta_{i,k-1}$ and lower levels. Therefore, for the first pre-selected levee-section LS_1, the failure probability at a given water level is

$$\begin{aligned} P(B_{1,1}) &= P_{f(LS_1)}(\eta_{1,1}) && \text{for } k = 1 \\ P(B_{1,k}) &= P(B_{1,k} \cap \overline{B}_{1,k-1} \cap \ldots \cap \overline{B}_{1,1}) = P_{f(LS_1)}(\eta_{1,k}) - P_{f(LS_1)}(\eta_{1,k-1}) && \text{for } k = 2, \ldots, N_1 \end{aligned} \quad (i = 1), \tag{8}$$

where event $B_{i,k}$ represents levee breaching at section LS_i for loading level $\eta_{i,k}$ ($i = 1$ in Eq. (8)), and the overbar denotes the opposite (non-failure) event. Since breaching event $B_{i,k}$ automatically excludes the occurrence of subsequent events $B_{i,k}$, …, B_{i,N_i}, the specification $\overline{B}_{i,k+1} \cap ... \cap \overline{B}_{i,N_i}$ is omitted in the definition of the $B_{i,k}$ event. Because events $B_{1,k}$ ($k = 1$, …, N_1) are mutually exclusive, the total probability $P(B_1)$ of breaching at levee section LS_1 (for any discrete water level) is

$$P(B_1) = P(B_{1,1} \cup ... \cup B_{1,N_1}) = \sum_{k=1}^{N_1} P(B_{1,k}), \tag{9}$$

while the residual probability $1 - P(B_1)$ is the no breach probability at the same section, i.e.

$$P(\overline{B}_1) = P(\overline{B}_{1,1} \cap ... \cap \overline{B}_{1,N_1}) = 1 - P(B_1) = 1 - \sum_{k=1}^{N_1} P(B_{1,k}). \tag{10}$$

In the previous analysis the attention was on the first upstream section of the pre-selected ones ($i = 1$). However, it can be extended to the others levee sections to assess the probability of a generic breach event $B_{i,k}$ at LS_i, with $i > 1$. To this end, the two following assumptions are made:

1) Considering the discretized levee as an in-series protection system, it is assumed that the hydraulic load is applied sequentially to the successive levee sections, one after another, from upstream to downstream, according to the natural temporal sequencing determined by the propagation of the flood wave in the river. In addition, it is assumed that one pre-selected levee section at a time is affected by the flood. Hence, the loading event is considered as acting separately on the successive pre-selected sections, as if they were ideally very far apart compared with the flood wave length. In reality, a flood event can simultaneously affect various river sections (with different water levels), depending on the distance between them, as well as the duration and the celerity of the flood wave. The maximum loading intensity (represented by the peak water level) decreases in the flow direction due to the attenuation effect inherent in flood wave propagation.

2) Although the occurrence of a breach event at a certain levee section does not eliminate the possibility that further breaches may happen in other sections during the same flood event, the occurrence of multiple breaches is ignored, based on the empirical observation that multiple breaches typically occur with low frequency during real floods. Breach events in different locations are therefore assumed mutually exclusive. Accordingly, in the case of a breach upstream, the conditional probability of additional breaches downstream is set to zero, as if the occurrence of a levee breach at a certain location caused a considerable drop in the water surface downstream, to the point of reducing to zero the risk of further breaches in the downstream sections. Consequently, the possible "failure states" of the levee system (with reference to the breach locations, including the no breach scenario) are reduced from 2^N to $N + 1$, with significant computational saving, especially for high values of N. This hypothesis makes the occurrence of a downstream breach dependent on the event that none of the upstream sections have breached earlier.

In view of the previous assumptions, the failure probability at section LS_i (with $i > 1$) deduced from the fragility function for fixed discrete water levels $\eta_{i,k}$ can be interpreted as conditional on the fact that no breach events occurred previously at the upstream sections.

Thus, breaching probability $P(B_{i,k})$ at water level $\eta_{i,k}$ is the joint probability of $B_{i,k}$ *and* $(\overline{B}_{i-1} \cap ... \cap \overline{B}_1)$, the latter expression meaning that none of the upstream sections LS_{i-1}, …, LS_1 breached previously. Event B_i denotes levee breaching at section LS_i regardless of the water stage that induces failure, thus it includes all events $B_{i,k}$ for $k = 1, \ldots, N_i$. The probability multiplication rule for dependent events yields

$$\begin{aligned} P(B_{i,k}) &= P(B_{i,k} \cap \overline{B}_{i,k-1} \cap ... \cap \overline{B}_{i,1} \cap \overline{B}_{i-1} \cap ... \cap \overline{B}_1) = \\ &= P(B_{i,k} \cap \overline{B}_{i,k-1} \cap ... \cap \overline{B}_{i,1} \,|\, \overline{B}_{i-1} \cap ... \cap \overline{B}_1) \cdot P(\overline{B}_{i-1} \cap ... \cap \overline{B}_1) \end{aligned} \quad \text{for } k = 1, ..., N_i \ (i = 2, ..., N), \tag{11}$$

and recalling that

$$P(\overline{B}_{i-1} \cap ... \cap \overline{B}_1) = 1 - \sum_{l=1}^{i-1} P(B_l) \quad \text{for } i = 2, ..., N \tag{12}$$

because events B_i are mutually exclusive, Eq. (11) becomes

$$\begin{aligned} P(B_{i,1}) &= P_{f(LS_i)}(\eta_{i,1}) \cdot \left[1 - \sum_{l=1}^{i-1} P(B_l) \right] && \text{for } k = 1 \\ P(B_{i,k}) &= \left[P_{f(LS_i)}(\eta_{i,k}) - P_{f(LS_i)}(\eta_{i,k-1}) \right] \cdot \left[1 - \sum_{l=1}^{i-1} P(B_l) \right] && \text{for } k = 2, ..., N_i \end{aligned} \quad (i = 2, ..., N). \tag{13}$$

The calculations proceed from upstream to downstream according to Eqs. (8) and (13). Finally, the probability that a breach occurs somewhere in the discretized levee system (at any discrete water level) is

$$P(B_1 \cup ... \cup B_N) = \sum_{i=1}^{N} P(B_i), \tag{14}$$

and the probability of the no breach scenario (i.e. the levee system withstands the water load caused by the design flood event without breaching) is

$$P(\overline{B}_1 \cap ... \cap \overline{B}_N) = 1 - P(B_1 \cup ... \cup B_N) = 1 - \sum_{i=1}^{N} P(B_i). \tag{15}$$

The cross-sections at which the boundary conditions are specified are usually gauged sections, where discharge or water level data are available. It is desirable that the failure probability of such boundary sections is equal to zero so as to avoid the interference between the breach outflow and the boundary conditions imposed. For this reason, the boundary sections are not included in the set of the pre-selected sections susceptible to breach. Moreover, the input flood hydrograph (of given return period) is typically obtained from the frequency analysis of historical data, which implies that breach events occurring upstream of the inflow section are not considered. The method is applied to either the right- or the left-bank levee of a river reach, thus neglecting the effects of potential levee breaches on the opposite side.

Ultimately, as a final outcome of the levee breach module, an ensemble of breach scenarios can be assembled, composed of breach events $B_{i,k}$ along with the no breach

scenario. Each breach scenario (labeled S_j hereinafter) is coupled with its probability $P(S_j)$, being $j = 1, \ldots, N_S$ a scenario index and $N_S = \sum_{i=1}^{N} N_i + 1$ the total number of scenarios, including the no breach scenario. Within this ensemble, the scenarios are ordered by breach location LS_i from upstream to downstream and, for each location, according to increasing $\eta_{i,k}$ values of the breach water level. Accordingly, breach event $B_{i,k}$ corresponds to breach scenario S_j, with $j = k$ for $i = 1$ and $j = k + \sum_{l=1}^{i-1} N_l$ for $i > 1$; $j = N_S$ refers to the no breach scenario. The probabilities associated with each breach scenario represent the scenario chances conditioned to a design flood event of given return period and constitute the weights to be assigned to the corresponding subsequent flooding for probabilistic flood inundation and hazard mapping.

Here Figure 4

2.2 Hydrodynamic model

Both deterministic and probabilistic flood hazard mapping require a hydrodynamic model capable of accurately simulating the flood dynamics and predict the key hydraulic variables involved in the flood hazard assessment (Teng et al., 2017). One-dimensional (1D) and two-dimensional (2D) models based on the shallow water equations are widely used in literature because of their ability to effectively simulate rapidly varied unsteady free surface flows, such as the flood wave routing in river channels (1D models) and the inundation of flood-prone areas (2D models), even in the presence of highly irregular topography (e.g., Horritt & Bates, 2002; Horritt et al., 2007; Tayefi et al., 2007; Aureli et al., 2008a; Pilotti et al., 2011; Pilotti et al., 2014; Vacondio et al., 2014; Costabile & Macchione, 2015). In the case of long river stretches and wide flood-prone areas, combined 1D-2D models can be very useful, ensuring a good compromise between model accuracy and computational efficiency (e.g., Dhondia and Stelling, 2002; Kamrath et al., 2006; Liu et al., 2015).

The hydrodynamic model used in this paper is a combined 1D-2D model in which the 1D and 2D modules are linked by means of lateral structures. In the event of breach opening, a weir-type formula is applied at these structures to model the flow exchange between the 1D and 2D computational domains through the levee breach.

The free software HEC-RAS v. 5.06 (Brunner, 2016a) is used for the numerical simulations due to its wide application for river flood modeling (e.g., Horritt & Bates, 2002; Tayefi et al., 2007; Cook & Merwade, 2009) and, recently, for 2D flood inundation modeling (see, for example, Quirogaa et al., 2016; Teng et al., 2017; Afshari et al., 2018). HEC-RAS solves the 1D De Saint Venant equations by the four-point Preissman implicit finite-difference scheme, and the full 2D shallow water equations by a semi-implicit, Eulerian-Lagrangian, finite volume scheme (Brunner, 2016b). An accurate description of the inundation process in the 2D flooding area is obtained through a sub-grid model (Brunner,

2016b), in which the bottom of the computational cells is not horizontal but follows the underlying terrain topography.

2.3. Spatial probability analysis model and probabilistic flood hazard mapping

After the probabilities of each breach scenario have been assessed using the probabilistic levee breach model previously described, the probability analysis of the hydrodynamic model results of the whole scenario ensemble allows producing the probabilistic flood inundation and hazard maps. Three different types of maps are used in this paper to represent the model outputs: 1) the probabilistic inundation extent map; 2) percentile maps of the key hydraulic quantities (such as maximum inundation depth, maximum flow velocity, and flooding arrival time) and of the flood hazard index; 3) the probabilistic maps of hazard levels defined according to a chosen flood hazard classification.

1) The probabilistic inundation extent map illustrates the areas expected to be inundated with a given probability, thereby providing, in each position of the flood-prone area, the probability of being flooded for the design flood event of given return period (e.g., Smemoe et al., 2007; Vorogushyn et al., 2010; Beven et al., 2015). The inundation probability P_I at each floodable location $\mathbf{x}$ is calculated by adding the probabilities of the breach scenarios inducing flooding in that location, that is

$$P_I(\mathbf{x}) = \sum_j P\left(S_j : h_{\max\, j}(\mathbf{x}) > 0\right), \tag{16}$$

in which $h_{\max j}(\mathbf{x})$ is the maximum inundation depth predicted at position $\mathbf{x}$ for scenario S_j.

2) A further outcome of the probability analysis is the spatial distribution in the floodable area of key flood quantities which are not exceeded with a given probability. This information is effectively visualized through percentile maps (see Vorogushyn et al., 2010). For instance, referring to inundation depth h, the X-percentile map of the maximum inundation depth $h_{\max}$ represents, for each floodable location $\mathbf{x}$, the local maximum value of the water depth which is exceeded with a probability of (100 – X)% for the selected design flood event of given return period, that is

$$h_{\max,\, \mathrm{X}\%}(\mathbf{x}) = \left[h_{\max}(\mathbf{x}) : P_{h_{\max}}(h_{\max};\mathbf{x}) = \mathrm{X}/100\right], \tag{17}$$

$P_{h_{\max}}(h_{\max};\mathbf{x})$ being the cumulative probability function of the stochastic variable $h_{\max}$ at position $\mathbf{x}$, defined as

$$P_{h_{\max}}(h_{\max};\mathbf{x}) = \sum_j P\left(S_j : h_{\max\, j}(\mathbf{x}) \le h_{\max}\right). \tag{18}$$

In addition, to provide summary information on the spatial variability of the central tendency of the probability distribution of $h_{\max}$, a probability-weighted average map can be generated as follows:

$$h_{\max,\, \mathrm{average}}(\mathbf{x}) = \sum_j P(S_j) \cdot h_{\max\, j}(\mathbf{x}). \tag{19}$$

3) The last result of the spatial probability analysis is the probabilistic assessment of the flood hazard in the floodable area. To this end, it is necessary beforehand to define a flood hazard classification, based on an index representative of the flood hazard intensity (e.g., Aureli et al., 2008b; Di Baldassarre et al., 2009b; Aronica et al., 2012; Mazzoleni et al., 2014). Several flood hazard classifications are present in literature and are adopted by government agencies for flood hazard management (e.g., ACER, 1988; DEFRA, 2006; Aronica et al., 2012); the flood hazard indexes are typically defined as a combination of inundation depth and flow velocity, sometimes dependent on the return period (Aronica et al., 2012). The classification suggested by DEFRA (2006) for people has been adopted in this paper. Such classification is based on flood hazard index *HR* defined as

$$HR = h \cdot (|\mathbf{v}| + 0.5) + DF \,, \tag{20}$$

h being the flooding depth (in m), $|\mathbf{v}|$ the magnitude of the flow velocity (in m/s), and *DF* a debris factor (which depends in turn on the flood depth and velocity, and on the land use), assumed equal to zero for simplicity. According to DEFRA (2006), flood hazard for people is categorized in four classes as low, moderate, significant, or extreme, depending on the fact that the maximum value of *HR* predicted belongs to the ranges $\Re_1 = (0, 0.75)$, $\Re_2 = [0.75, 1.25)$, $\Re_3 = [1.25, 2.5)$, or $\Re_4 = [2.5, +\infty)$, respectively (see Figure 5). The probabilistic flood hazard maps can then provide, for the design flood event of given return period, the spatial distribution of the probability of each flood hazard class, i.e. the probability of each position $\mathbf{x}$ to fall in the different flood hazard classes, that is

$$P_{\Re_m}(\mathbf{x}) = \sum_j P(S_j : HR_{\max j}(\mathbf{x}) \in \Re_m) \,, \tag{21}$$

in which *m* is an index referring to the hazard class, and $HR_{\max j}(\mathbf{x})$ is the maximum value of *HR* evaluated at position $\mathbf{x}$ for the *j*-breach scenario. Accordingly, a probabilistic flood hazard map can be drawn for each hazard class considered. In addition, the maximum value of the flood hazard level corresponding to a given probability can be calculated in each location according to Eqs. (17) and (18) modified by replacing $h_{\max}$ with $HR_{\max}$. Percentile maps of the flood hazard index can then be generated. Similarly, a probability-weighted average flood hazard map can be obtained adapting Eq. (19).

It is worth noting that the flood hazard classification can be adapted to the jeopardized element being considered (see ACER, 1988). With respect to this, it should be borne in mind that various stability criteria have been proposed in literature for persons, buildings, and vehicles (see Milanesi et al., 2016; Milanesi et al., 2018; Martínez-Gomariz et al., 2018, respectively).

Here Figure 5

2.4. Limitations of the method

The implications of the main assumptions of the method are discussed in this subsection.

1) The method requires that a design flood event of given return period be assigned. Hence the results of the flood hazard analysis are conditional on a hydrologic load of given frequency of occurrence. However, this not preclude the application of the method to hydrological events of different return periods. In this regard, Vorogushyn et al. (2010) obtained probabilistic inundation hazard maps, and Winter et al. (2018) estimated monetary damages caused by floods for different return periods. Incidentally, flood events of different severity must be taken into account when the criterion chosen for flood hazard classification includes the return period (Aronica et al., 2012). Using a different approach, Hall et al. (2003), Dawson et al. (2005), and Dawson and Hall (2006) combined the levee fragility function with the probability density function of the hydraulic loading in order to estimate the unconditional probability of failure of selected defense sections, thereby taking into account all relevant hydrologic scenarios in flood risk analysis in a probabilistic way. In the method proposed in this paper, a design flow hydrograph is imposed as an upstream boundary condition for the selected return period. The influence of uncertainty in boundary conditions on flood inundation predictions was analyzed in detail by Pappenberger et al. (2006) and Domeneghetti et al. (2013).

2) Only levee failure due to piping is considered in the method. However, the analysis of the levee reliability can easily be extended to other failure mechanisms, even multiple ones, by adequately adapting the fragility functions (Apel et al., 2006; Dawson and Hall, 2006; Vorogushyn et al., 2010; Marijnissen et al., 2019). It is worth noting that in the case of complex probabilistic reliability procedures involving different failure mechanisms, the Monte Carlo method is a general feasible solution, albeit computationally expensive (Vorogushyn et al., 2009).

3) Only levee porosity is treated as a stochastic variable in the reliability function adopted for piping (Khilar et al., 1985). Indeed, porosity is among the most uncertain parameters in the levee reliability assessment. However, more complex piping models and various empirical reliability functions can be used (Vorogushyn et al., 2009), even considering several parameters as stochastic. The geotechnical and geometrical properties of the levee sections, excluding levee porosity, are considered as deterministic in this paper, as well as the other model inputs and parameters. The influence of the uncertainty associated with such elements on flood inundation predictions has been extensively analyzed in literature (see Merwade et al., 2008). In particular, Sanyal (2017) recently developed a probabilistic methodology for dealing with the effect of uncertainty in levee heights on the inundation pattern.

4) Breach development is assumed instantaneous, and breach length and shape are fixed a priori since the focus of the paper is on the effects of breach location and time. A plausible value of the breach width could generally be derived from the historical field data concerning the study area, when available. Alternatively, simple empirical models proposed in literature could be used to estimate the breach growth rate and the final breach width (IMPACT, 2005; Dawson et al., 2005; Dawson and Hall, 2006). However, breach geometry characteristics are highly uncertain, and their correct estimation is important to accurately predict flooding extent (Mazzoleni et al., 2014). For this reason, several studies have dealt with the effect of uncertainties in breach size (Di Baldassarre et al., 2009; Vorogushyn et al., 2010;

Domeneghetti et al., 2013; Mazzoleni et al., 2017) and breach development (Vorogushyn et al., 2011) on flood hazard mapping. When an empirical frequency distribution of breach width can be computed, different breach lengths (with the associated frequencies) could be considered for each breach location and time (Apel et al., 2006; Vorogushyn et al., 2010; Mazzoleni et al., 2014). Accordingly, the number of breach scenarios to be taken into account may increase considerably, along with the computational effort required.

5) The hydraulic load on a river levee system varies in time during a flood event. The method assumes that levee breaching can only occur during the rising stage of the flood (i.e. for increasing water levels). Moreover, hydraulic loading is assumed to act sequentially and separately on the successive pre-selected levee sections from upstream to downstream, according to the natural temporal sequencing determined by the propagation of the flood wave in the river. Uncertainty in the loading conditions on a levee system has been extensively investigated in literature (Apel et al., 2004; Dawson et al., 2005, Dawson and Hall, 2006; Hall and Solomatine, 2008; Lendering et al., 2018; Winter et al., 2018). However, the temporal component of load sequencing is usually neglected, i.e. all sections of the defense system are assumed to be subject to the same peak hydraulic load at almost the same time (Hall et al., 2003; Dawson et al., 2005; Harvey et al, 2014).

6) Multiple breach scenarios are ignored, i.e. the probability that two or more breaches occur at different locations during the same flood event is neglected, based on the empirical observation that multiple breaches are rather infrequent in real flood events. Indeed, the occurrence of an upstream breach may significantly reduce downstream water levels and, consequently, the conditional probability of failure at downstream levee sections. In view of the present and previous assumption 5), breach scenarios characterized by different breach locations and failure times are considered as mutually exclusive. On the other hand, multiple failure states are usually treated as independent in literature (Hall et al., 2003; Dawson et al., 2005; Gouldby et al., 2008; Harvey et al., 2014), which means that the hydraulic interactions between breach events occurring during the same flood event are neglected. Including multiple breaches in the analysis can imply that a large number of combinations of breach locations and possibly times should be considered, especially for long levee reaches described with many cross-sections, thus requiring a prohibitive computational effort (Dawson et al., 2005). Dawson and Hall (2006) and Harvey et al. (2014) developed efficient flood risk methodologies to reduce this problem.

3 Case study

The probabilistic method is applied to a 96 km reach located in the central portion of the Po River (northern Italy), between the Cremona and Borgoforte gauging stations (Figure 6). Along this reach, the river is braided, with wide and flat floodplains, and the average riverbed slope is approximately 0.2 m per km; five main tributaries on the right-hand side and one on the left-hand side flow into the river. A levee system provides protection to the adjacent flood-prone areas on both the right and left banks. Only breach events on the right-hand side levee system are considered in this paper. In the case of this type of event, a densely-urbanized area of approximately 1900 km^2 is potentially exposed to flooding. Only failures caused by piping are considered here, since the historical records show that this breaching mechanism has been the primary cause of levee failures in this specific reach in the last two centuries (Turitto et al., 2010; Mazzoleni et al., 2015). It is worth noting that most of

609 the recent levee failures which caused large flooding in northern Italy were not triggered by
610 overtopping, but were likely induced by internal erosion due to seepage phenomena (e.g.,
611 Serchio River in 2009, Bacchiglione River in 2010, Secchia River in 2014).

612

613 *Here Figure 6*

614

615 The database from the Italian Agency for the Po River Management (AIPO) was used
616 to collect sixty-one cross-sections between the main levees for the reach analyzed (Figure 6);
617 these derive from a ground survey and have an average distance of 1.6 km. The right-hand
618 side levee system was discretized according to these cross-sections, where the fragility
619 functions for piping were evaluated. In addition to these 61 river cross-sections, a 2 m
620 resolution digital terrain model (DTM) based on LiDAR data is available which covers most
621 of the floodable area of interest. Additional 5 m and 20 m resolution DTMs, obtained from
622 vector contour lines, were used to complete the topographic description of the flood-prone
623 area where gaps in the 2 m DTM were present. Between the main levees of the Po River, the
624 LiDAR data were combined with a sonar survey covering the submerged portion of the main
625 channel to enhance the description of the river bed geometry.

626 Supplementary cross-sections extracted from the DTM at an average distance of
627 100 m were added to the 61 cross-sections mentioned above to accurately reproduce the river
628 geometry in the 1D model. The model was calibrated against a severe flood event (of
629 approximately 50-year return period) which had occurred in October 2000. To this end, the
630 inflow hydrograph at the Cremona gauging station, estimated on the basis of the recorded
631 water levels by using a reliable rating curve, was imposed at the upstream boundary, while
632 the stage hydrograph recorded at the Borgoforte gauging station was used as downstream
633 boundary condition. The calibration was performed by adjusting the Manning coefficients of
634 the main channel and of the floodplains to satisfactorily reproduce the water levels recorded
635 at the intermediate Boretto gauging station (Figure 6). The PEST suite (Doherty, 2010) was
636 adopted to automate the calibration procedure and it returned roughness values of 0.045 and
637 0.1 $m^{-1/3}s$ for the main channel and the floodplains, respectively. These estimates agree with
638 the ones obtained in previous studies on the same river reach (e.g., Mazzoleni et al., 2014 and
639 2015).

640 In the HEC-RAS hydrodynamic model, lateral structures (which act as internal
641 boundary elements) were used to represent the right-hand side levee and link the 1D river
642 reach to the 2D floodable area in the event of levee failure. A weir-type formula was adopted
643 to model the flow exchange between the two computational domains through the breach.
644 Based on Brunner (2016a), the dimensional weir coefficient C was set at 1.1 $m^{1/2}/s$, which
645 corresponds to a conventional dimensionless discharge coefficient $\mu = C/(2g)^{1/2}$ equal to
646 approximately 0.25, g being the acceleration due to gravity.

647 The flood-prone area was discretized through a mixed structured-unstructured 2D
648 mesh. It was built starting from a 50 m × 50 m structured grid that was then refined near the
649 main topographic singularities by means of unstructured cells. Breaklines were inserted along
650 the topographic elements that could significantly affect the flood propagation (such as levees
651 or road embankments), with the aim of forcing the cell boundaries to follow these lines. A

total of 887993 cells and 940969 nodes were obtained in the 2D computational domain, where the Manning roughness coefficient was assumed to vary spatially with the land use reported in the Corine Land Cover (2012) database. Roughness values in the range from 0.02 to 0.3 $m^{-1/3}s$ were set according to the land cover type (Chow, 1959).

The numerical flood simulations were performed imposing a 100-year return period synthetic design hydrograph (Maione et al., 2003) at the upstream boundary (Cremona gauging station) of the 1D hydrodynamic model (Figure 7a). A reliable rating curve was specified at the downstream end of the model (Borgoforte gauging station; Figure 7b). The tributary flow contributions were neglected, thus assuming that the flood event affected the main stem only. A preliminary 1D flood routing simulation was performed without levee breaches in order to predict the maximum water levels at the 61 primary cross-sections and pre-select the locations where the levee system has the greatest chance of failing.

Here Figure 7

A rectangular-shaped breach of constant width and depth was assumed in the flooding simulations, regardless of the failure location. The breach width was set at 100 m, which is the median value of the historical data concerning breaches due to piping in the right-hand side levee of the river reach considered (Turitto et al, 2010; Mazzoleni et al., 2015). The levee failure was triggered by the reaching of prescribed water levels (determined on the basis of the probabilistic levee breach model), and the breach opening was assumed to instantaneously reach the landside natural ground level, since the breach developing time is reasonably shorter than the overall flood duration.

The variable time stepping algorithm, recently implemented in HEC-RAS (Brunner, 2018) and based on the Courant stability condition, was used to improve the model's stability and reduce the computational burden of the numerical simulations. A simulation time of approximately 5 h is required on average on a desktop computer with an Intel Xeon processor (3.6 Ghz) and 16 GB of RAM to simulate a physical 10 d flooding on a mesh with 887993 cells. Differences between the scenarios depend on the specific features of the predicted inundation dynamics and, mainly, on the flooding extent.

4 Results

This section presents the results obtained by applying the probabilistic method to the case study described in the previous section.

The first key result is provided by the probabilistic levee breach module and consists in the assessment of the breach scenario probabilities, i.e. the levee failure probability for piping at selected locations and times. Fourteen of the 61 sections used to discretize the levee system are potentially susceptible to failure for the 100-year return period flood event ($N = 14$), and represent the locations most critical to piping. After discretization of the corresponding 14 fragility curves based on 5%-probability intervals (see Figure 4), 26 breach scenarios can be defined ($N_S = 26$), including the no breach one. Breach scenarios with estimated probability lower than the 0.5% threshold are disregarded for simplicity. Figure 8

shows the 14 "pre-selected" potential breach locations; the probabilities reported are calculated by adding the probabilities of all the breach scenarios (characterized by different failure times, corresponding to different flow conditions in the river) defined at the same location. Of the 14 breach positions six are located in the central portion of the river reach, while the remaining are concentrated in the downstream portion. It is worth noting that the locations agree fairly well with the positions of the main sand boils observed during the severe flood events which occurred in the Po River in 1994 and 2000 (see Coratza, 2004; Mazzoleni et al., 2014). Conversely, no levee breaching induced by piping is expected in the upstream part of the reach, where the levee exhibits a high resistance against piping for the flood event considered. The highest breach probabilities are estimated for the levee cross-sections with smaller width, or in which the landside levee toe is lower than the riverside floodplain (see Figure 2b). The sum of all the breach scenario probabilities, indicating the chance that a breach occurs somewhere in the levee system, is approximately 65%. The residual probability of approximately 35% refers to the case of no occurrence of breaches along the levee system for the design flood event considered. However, these values are influenced by the assumption of neglecting multiple breach scenarios. In the case study analyzed (see Figure 8), the joint probability that levee section LS_1 fails at the peak water level and later section LS_2 breaches, again at the peak water level (obviously influenced by the breaching at LS_1), is equal to approximately 0.15%. This result confirms that the individual impact on the total probability of high order scenarios characterized by two (or even more) multiple breaches is not particularly significant, at least in the case study considered.

Here Figure 8

After simulating the inundations related to each breach scenario through the hydrodynamic model, the different maps listed in Section 2.3 can be obtained through the probability analysis of the numerical results. A first outcome of this analysis is the 1-in-100 year flood probabilistic map of the inundation extent shown in Figure 9. This map illustrates the areas that can be expected to be inundated with different probabilities for the design flood event with a recurrence interval of 100 years. The inundation probabilities reach the highest values (greater than 25%) in the eastern part of the flood-prone area because different breach scenarios determine predicted flooded areas overlapping to a large extent. Moreover, distinct circumscribed flooded areas are clearly recognizable, due to the presence of the levee systems of the main right-hand bank tributaries of the Po River, which constitute barriers to the flow in the floodable plain. The borders of the flooded areas are distinctly defined by the topographic obstacles, where they affect the evolution of the inundation process. Conversely, wherever the inundation extent is determined by the natural mild terrain slope, the borders of the inundated area appear blurred, with a gradual decrease to zero in inundation probability.

Here Figure 9

Another significant result of the spatial probability analysis is the distribution of selected percentiles of the maximum inundation depth in the flood-prone area for the design flood event of given return period. This information can effectively be represented by percentiles maps. As an example, panels a-c in Figure 10 show the 1-in-100 year flood maps of the 75th, 90th, and 99th percentile of the maximum inundation depth for the case study analyzed. Percentile maps provide a more comprehensive characterization of the probability distribution of the variable represented in comparison with a concise probability-weighted average map (see Figure 10d), where the estimated mean values at each location cannot be realistically attributed to any breach scenario. It can be noted from Figure 10 that both the extent of the flooded area and the maximum inundation depth at a selected position increase for increasing percentile, as expected. Moreover, the 99th percentile map (Figure 10c) shows that water depths up to approximately 10 m might occur in the central portion of the flood-prone area, due to the combined presence of depressed lands and high embankments. Similar maps can be produced for any other significant hydraulic quantity, such as maximum flow velocity or flood arrival time. These maps are not shown here for the sake of brevity.

Here Figure 10

The ultimate outcome of post-processing the simulation results is represented by probabilistic flood hazard maps. Figure 11 shows 1-in-100 year flood probabilistic maps that depict the spatial distribution of the probability of the four flood hazard levels (low, moderate, significant, and extreme; see Figure 5) identified by DEFRA (2006) for the 100-year return period design flood event. The flood hazard level is evaluated on the basis of the predicted maximum value of index *HR* defined in Eq. (20). It should be noted that a specific location in the flood-prone area can fall in different hazard classes at the same time, with different probabilities. Figure 11d shows that the extreme flood hazard level occurs with significant probability (10-15%) in the central region of the flood-prone area, where the highest values of the maximum water depth are expected.

Here Figure 11

Probabilistic flood hazard maps can also be represented in terms of percentile maps, as for the probabilistic inundation maps in Figure 10. Figure 12a-c shows the 75th, 90th, and 99th percentile maps of the maximum value of the flood hazard index for the design flood event of 100-year return period. For each location, the flood hazard intensity expected to be exceeded with 25%, 10%, and 1% probability, respectively, can be extracted from these maps. Alternatively, the areas characterized by the highest values of the flood hazard index (or by values greater than a fixed threshold) can easily be identified for a given percentile. This probabilistic information can be very useful for the assessment and management of the flood risk in the area analyzed. Finally, Figure 12d shows the probability-weighted average map of the maximum value of the hazard index. Such a map appears to be very similar to the flood hazard maps usually generated in the conventional flood hazard analyses, and provides

777 a concise “average” probabilistic assessment of the flood hazard; it can thus be adopted as a
778 first approach for land-planning and flood-risk management purposes.

779

780 *Here Figure 12*

781

782 **5 Conclusions**

783 A probabilistic multi-module method for the assessment of the flood hazard due to
784 piping-induced levee failures in flood-prone areas has been proposed in this paper. The
785 concept of fragility function (which describes the vulnerability of a levee system at a selected
786 section) and the probability multiplication rule for dependent events were employed to
787 estimate breach scenario probabilities, representative of the uncertainty of levee breaching at
788 selected locations and times, conditioned to a design flood event of given return period.
789 Fragility functions for piping were obtained for the cross-sections of a discretized levee
790 system through a reliability analysis based on a suitable performance index. Only levee
791 porosity was considered as a stochastic variable in assessing this index.

792 Attention was focused on the uncertainty about breach location and failure time due to
793 the significant influence that these factors have on the dynamics of the subsequent inundation
794 and on the delimitation of the flooded areas. An ensemble of potential levee failure scenarios
795 was pre-selected on the basis of a preliminary hydrodynamic simulation performed by
796 assuming no levee breaches along the river. Thanks to the preliminary identification of the
797 sections where the levee is more susceptible to breach, the method offers the advantage of
798 requiring fewer simulation runs in comparison with most probabilistic methods proposed in
799 literature, typically based on computationally expensive Monte Carlo procedures. Moreover,
800 since the method assigns a probability to each breach scenario and subsequent flooding, it
801 allows the quantification of the uncertainty of the hydraulic variables involved in the flood
802 hazard assessment, thus providing more comprehensive information compared to the
803 conventional deterministic methods. Indeed, the deterministic methods are typically based on
804 a single “optimum” scenario and, in the best cases, are accompanied by a sensitivity analysis
805 on the key parameters.

806 The main assumptions and limitations of the proposed method are recalled below.
807 1) The analysis was performed for a design flood event of given return period. 2) Only piping
808 was considered among the different levee breach mechanisms. 3) Topographic and
809 hydrologic data were treated in a deterministic way. Only levee porosity was considered as a
810 stochastic variable in the derivation of the fragility functions for piping. 4) The geometric
811 characteristics of the breaches were treated as deterministic and fixed a priori; the breach was
812 assumed to occur instantaneously. 5) It was assumed that levee failure could only occur
813 during the rising stage of the flood wave, and that the hydraulic load was applied separately
814 to the successive pre-selected levee sections from upstream to downstream. 6) Multiple
815 breach scenarios were neglected. Due to its relevance, this specific topic ought to be further
816 analyzed, and will indeed be investigated in a future study.

The method was applied to a 96 km reach of the central portion of the Po River (northern Italy) to verify its effectiveness in probabilistic inundation and flood hazard mapping. The spatial probability analysis conducted on the numerical results of the hydrodynamic model allows the following maps to be generated (for a design flood event of given return period): 1) the probabilistic inundation extent map; 2) percentile maps of the key hydraulic quantities (such as the maximum inundation depth and velocity, and the flooding arrival time) and of the flood hazard index; 3) the probabilistic map of the hazard levels defined according to a chosen classification. Unlike conventional deterministic maps, which typically define the flooded area boundaries on the basis of a "best" scenario, the probabilistic inundation extent maps identify the areas that are expected to be inundated with different probabilities. Similarly, unlike conventional maps of the maximum inundation depth, which represent an inundation pattern derived from a single scenario, percentile probability maps take into account different possible flood scenarios. For each location in the flood-prone area they provide the maximum water depth value which it is expected not to be exceeded with fixed probabilities. In addition, interpercentile ranges can be extracted for each location from different percentile maps. Similar considerations apply to the percentile maps of flood hazard. Probabilistic flood hazard maps can also represent the spatial distribution of the probability of each hazard level defined in the classification adopted. The flood hazard assessment is based on an ensemble of breach scenarios (along with the associated probabilities), each producing different inundation effects, so distinct flood hazard levels can be predicted in the same location, with different probabilities.

Probabilistic flood hazard mapping does have the drawback that results cannot be exhaustively represented in concise thematic maps as in the deterministic analyses. However, incorporating uncertainty (in terms of probability) in flood hazard assessment supports more informed and flexible management and planning decisions. The information concerning probability is indeed an additional useful element to better orient land-use planning strategies and structural interventions for flood hazard mitigation, which can be adequately designed on the basis of the risk propensity of the floodable areas. Moreover, the probabilistic analysis helps differentiate between situations characterized by similar "average" flood hazard conditions and carefully use the economic resources available by concentrating preventive measures in the areas where significant flood hazard is predicted with the highest probability in the first instance. Finally, effective communication of the uncertainty affecting the results contributes to forming a correct perception of risk in society.

Acknowledgments

The Co-Editor (J. Hall), S. Vorogushyn, and the two anonymous reviewers are kindly acknowledged for their valuable suggestions and thorough appraisal, which have greatly contributed to the improvement of the paper.

The cross-sectional data of the Po River are available on the Italian Interregional Agency for the Po River (AIPo) website on: http://geoportale.agenziapo.it/cms/index.php?option=com_content&view=article&id=129&Itemid=105.

858 The topographic data of the flood prone area can be accessed on the National
859 Geoportal of the Italian Ministry of Environment and Protection of Land and Sea on:
860 http://www.pcn.minambiente.it/mattm/en/data-distribution-service-pst/.

861 All data used in this paper can be accessed in a public repository on:
862 https://doi.org/10.6084/m9.figshare.9729251.v3.

863 **Appendix A**

864 In the case study shown in the paper, a triangular probability density distribution is
865 assumed for levee porosity, with n ranging from $n_{\min}$ to $n_{\max}$ (see Mazzoleni et al., 2015), i.e.

866
$$f_n(n) = \begin{cases} 0 & \text{if } n < n_{\min} \\ p_0 \dfrac{n - n_{\min}}{n_0 - n_{\min}} & \text{if } n_{\min} \le n \le n_0 \\ p_0 \left(1 - \dfrac{n - n_0}{n_{\max} - n_0} \right) & \text{if } n_0 < n \le n_{\max} \\ 0 & \text{if } n > n_{\max} \end{cases}, \qquad \text{(A1)}$$

867 where p_0 denotes the probability density corresponding to the modal value n_0
868 ($n_{\min} < n_0 < n_{\max}$) and is equal to $2(n_{\max} - n_{\min})^{-1}$ so that $\int_{n_{\min}}^{n_{\max}} f_n(n)\,dn = 1$. Substituting Eqs.
869 (A1), (6), and (7) in Eq. (5) yields

870
$$f_G(G) = \begin{cases} 0 & \text{if } G < G_{\min} \\ p_0 \left[1 - \dfrac{1}{n_{\max} - n_0} \left(\dfrac{C}{G + \frac{\eta}{L} + C} - n_0 \right) \right] \dfrac{C}{\left(G + \frac{\eta}{L} + C \right)^2} & \text{if } G_{\min} \le G \le G_0 \\ \dfrac{p_0}{n_0 - n_{\min}} \left(\dfrac{C}{G + \frac{\eta}{L} + C} - n_{\min} \right) \dfrac{C}{\left(G + \frac{\eta}{L} + C \right)^2} & \text{if } G_0 < G \le G_{\max} \\ 0 & \text{if } G > G_{\max} \end{cases}, \qquad \text{(A2)}$$

871 with $G_{\min} = G(n_{\max})$, $G_0 = G(n_0)$, and $G_{\max} = G(n_{\min})$. The cumulative probability of the
872 stochastic variable G can be obtained from Eq. (A2) by integration:

873
$$P_G(G) = \begin{cases} 0 & \text{if } G < G_{\min} \\ p_0 C \left(1 + \dfrac{n_0}{n_{\max} - n_0} \right) \left(\dfrac{1}{G_{\min} + \frac{\eta}{L} + C} - \dfrac{1}{G + \frac{\eta}{L} + C} \right) - \dfrac{p_0 C^2}{2(n_{\max} - n_0)} \left[\dfrac{1}{\left(G_{\min} + \frac{\eta}{L} + C \right)^2} - \dfrac{1}{\left(G + \frac{\eta}{L} + C \right)^2} \right] & \text{if } G_{\min} \le G \le G_0 \\ P_{G_0} + p_0 C \dfrac{n_{\min}}{n_0 - n_{\min}} \left(\dfrac{1}{G + \frac{\eta}{L} + C} - \dfrac{1}{G_0 + \frac{\eta}{L} + C} \right) - \dfrac{p_0 C^2}{2(n_0 - n_{\min})} \left[\dfrac{1}{\left(G + \frac{\eta}{L} + C \right)^2} - \dfrac{1}{\left(G_0 + \frac{\eta}{L} + C \right)^2} \right] & \text{if } G_0 < G \le G_{\max} \\ 1 & \text{if } G > G_{\max} \end{cases}, \qquad \text{(A3)}$$

874

where P_{G_0} indicates the cumulative probability at $G = G_0$. It can easily be verified that P_G is equal to one for $G = G_{\max}$. P_G calculated at $G = 0$ according to Eq. (A3) provides the probability $P_G(G \le 0 \mid \eta)$ of levee failure as a function of the hydraulic load η, which represents the fragility function $P_f(\eta)$ at a selected section, that is

$$P_f(\eta) = \begin{cases} 0 & \text{if } 0 < G_{\min} \\ p_0 C\left(1 + \dfrac{n_0}{n_{\max} - n_0}\right)\left(\dfrac{1}{G_{\min} + \dfrac{\eta}{L} + C} - \dfrac{1}{\dfrac{\eta}{L} + C}\right) - \dfrac{p_0 C^2}{2(n_{\max} - n_0)}\left[\dfrac{1}{\left(G_{\min} + \dfrac{\eta}{L} + C\right)^2} - \dfrac{1}{\left(\dfrac{\eta}{L} + C\right)^2}\right] & \text{if } G_{\min} \le 0 \le G_0 \\ P_{G_0} + p_0 C \dfrac{n_{\min}}{n_0 - n_{\min}}\left(\dfrac{1}{\dfrac{\eta}{L} + C} - \dfrac{1}{G_0 + \dfrac{\eta}{L} + C}\right) - \dfrac{p_0 C^2}{2(n_0 - n_{\min})}\left[\dfrac{1}{\left(\dfrac{\eta}{L} + C\right)^2} - \dfrac{1}{\left(G_0 + \dfrac{\eta}{L} + C\right)^2}\right] & \text{if } G_0 < 0 \le G_{\max} \\ 1 & \text{if } 0 > G_{\max} \end{cases} \quad \text{(A4)}$$

References

ACER Technical Memorandum No. 11 (1988). *Downstream Hazard Classification Guidelines*. Denver, Colorado: U.S. Department of the Interior, Bureau of Reclamation.

Afshari, S., Tavakoly, A. A., Rajib, M. A., Zheng, X., Follum, M. L., Omranian, E., & Fekete, B. M. (2018). Comparison of new generation low-complexity flood inundation mapping tools with a hydrodynamic model. *Journal of Hydrology*, *556*, 539–556. https://doi.org/10.1016/j.jhydrol.2017.11.036

Apel, H., Thieken, A. H., Merz, B., & Blöschl, G. (2004). Flood risk assessment and associated uncertainty. *Natural Hazards and Earth System Science*, *4*(2), 295–308. https://doi.org/10.5194/nhess-4-295-2004

Apel, H., Thieken, A. H., Merz, B., & Blöschl, G. (2006). A probabilistic modelling system for assessing flood risks. *Natural Hazards*, *38*(1–2), 79–100. https://doi.org/10.1007/s11069-005-8603-7

Apel, H., Merz, B., & Thieken, A. H. (2009). Influence of dike breaches on flood frequency estimation. *Computers & Geosciences*, *35*(5), 907–923. https://doi.org/10.1016/j.cageo.2007.11.003

Aronica, G., Bates, P. D., & Horritt, M. S. (2002). Assessing the uncertainty in distributed model predictions using observed binary pattern information within GLUE. *Hydrological Processes*, *16*(10), 2001–2016. https://doi.org/10.1002/hyp.398

Aronica, G. T., Candela, A., Fabio, P., & Santoro, M. (2012). Estimation of flood inundation probabilities using global hazard indexes based on hydrodynamic variables. *Physics and Chemistry of the Earth, Parts A/B/C*, *42*, 119–129. https://doi.org/10.1016/j.pce.2011.04.001

Aureli, F., & Mignosa, P. (2004). Flooding scenarios due to levee breaking in the Po River. *Proceedings of the Institution of Civil Engineers - Water Management*, *157*(1), 3–12. https://doi.org/10.1680/wama.2004.157.1.3

Aureli, A., Maranzoni, A., Mignosa, P., & Ziveri, C. (2006a). *Flood hazard mapping by means of fully-2D and quasi-2D numerical modeling: a case study*. Paper presented at 3rd International Symposium on Flood Defence, Nijmegen, The Netherlands.

Aureli F., Maranzoni A., Mignosa P., & Ziveri, C. (2006b). *Fully-2D and quasi-2D modeling of flooding scenarios due to embankment failure.* Paper presented at River Flow 2006, 3rd International Conference on Fluvial Hydraulics, Lisbon, Portugal.

Aureli, F., Maranzoni, A., Mignosa, P., & Ziveri, C. (2008a). A weighted surface-depth gradient method for the numerical integration of the 2D shallow water equations with topography. *Advances in Water Resources*, *31*(7), 962–974. https://doi.org/10.1016/j.advwatres.2008.03.005

Aureli F., Maranzoni A., Mignosa P., & Ziveri, C. (2008b). *2D numerical modelling for hydraulic hazard assessment: a dam-break case study*. Paper presented at River Flow 2008, 4th International Conference on Fluvial Hydraulics, Ceşme, Turkey.

Bales, J. D., & Wagner, C. R. (2009). Sources of uncertainty in flood inundation maps. *Journal of Flood Risk Management*, *2*(2), 139–147. https://doi.org/10.1111/j.1753-318X.2009.01029.x

Bates, P. D., Horritt, M. S., Aronica, G., & Beven, K. (2004). Bayesian updating of flood inundation likelihoods conditioned on flood extent data. *Hydrological Processes*, *18*(17), 3347-3370. https://doi.org/10.1002/hyp.1499

Beven, K., Lamb, R., Leedal, D., & Hunter, N. (2015). Communicating uncertainty in flood inundation mapping: a case study. *International Journal of River Basin Management*, *13*(3), 285–295. https://doi.org/10.1080/15715124.2014.917318

Brunner, G. W. (2016a). *HEC-RAS, River Analysis System, 2D Modeling User's Manual Version 5.0.* Davis, CA: US Army Corps of Engineers, Institute for Water Resource, Hydrologic Engineering Center.

Brunner, G. W. (2016b). *HEC-RAS, River Analysis System, Hydraulic Reference Manual*. Davis, CA: US Army Corps of Engineers, Institute for Water Resource, Hydrologic Engineering Center.

Brunner, G. W. (2018). *HEC-RAS, River Analysis System, Supplemental User's Manual Version 5.0.4.* Davis, CA: US Army Corps of Engineers, Institute for Water Resource, Hydrologic Engineering Center.

Camici, S., Barbetta, S., & Moramarco, T. (2017). Levee body vulnerability to seepage: the case study of the levee failure along the Foenna stream on 1 January 2006 (central Italy). *Journal of Flood Risk Management*, *10*(3), 314–325. https://doi.org/10.1111/jfr3.12137

Chow, V.T. (1959) *Open-channel hydraulics*. New York: McGraw-Hill.

Cook, A., & Merwade, V. (2009). Effect of topographic data, geometric configuration and modeling approach on flood inundation mapping. *Journal of Hydrology*, *377*(1–2), 131–142. https://doi.org/10.1016/j.jhydrol.2009.08.015

Coratza, L. (2004). *Aggiornamento del catasto delle arginature maestre del fiume Po [Cadastre update of the main levees of the Po River]*. Parma: Po Basin Authority (in Italian).

Corine Land Cover (2012). https://land.copernicus.eu/pan-european/corine-land-cover/clc-2012

Costabile, P., & Macchione, F. (2015). Enhancing river model set-up for 2-D dynamic flood modelling. *Environmental Modelling & Software*, *67*, 89–107. https://doi.org/10.1016/j.envsoft.2015.01.009

Covelli, C. (2006). *Sulla formazione di brecce nei rilevati arginali: implicazioni relative alla protezione idraulica del territorio [Levee breaching and hydraulic hazard mitigation]* (Doctoral dissertation). Retrieved from fedOA (http://www.fedoa.unina.it/id/eprint/703). Naples, Italy: Università degli Studi di Napoli "Federico II" (in Italian).

CRED (2018a). *Natural Disasters 2017*. Brussels: Centre for Research on the Epidemiology of Disasters.

CRED (2018b). *Economic Losses, Poverty & Disasters 1998-2017*. Brussels: Centre for Research on the Epidemiology of Disasters.

Dawson, R., Hall, J., Sayers, P., Bates, P., & Rosu, C. (2005). Sampling-based flood risk analysis for fluvial dike systems. *Stochastic Environmental Research and Risk Assessment*, *19*(6), 388–402. https://doi.org/10.1007/s00477-005-0010-9

Dawson, R., & Hall, J. (2006). Adaptive importance sampling for risk analysis of complex infrastructure systems. *Proceedings of the Royal Society A: Mathematical, Physical and Engineering Sciences*, *462*(2075), 3343–3362. https://doi.org/10.1098/rspa.2006.1720

de Moel, H., van Alphen, J., & Aerts, J. C. J. H. (2009). Flood maps in Europe – methods, availability and use. *Natural Hazards and Earth System Sciences*, *9*, 289–301. https://doi.org/10.5194/nhess-9-289-2009

DEFRA Environment Agency (2006). *Flood Risks to People* (FD2321/TR2 Guidance Document). London: Department for Environment, Food and Rural Affairs.

Di Baldassarre, G, Castellarin, A, & Brath, A. (2009a). Analysis on the effects of levee heightening on flood propagation: some thoughts on the River Po. *Hydrological Sciences Journal*, *54*(6), 1007–1017. https://doi.org/10.1623/hysj.54.6.1007

Di Baldassarre, G., Castellarin, A., Montanari, A., & Brath, A. (2009b). Probability-weighted hazard maps for comparing different flood risk management strategies: a case study. *Natural Hazards*, *50*(3), 479–496. https://doi.org/10.1007/s11069-009-9355-6

Di Baldassarre, G., Schumann, G., Bates, P. D., Freer, J. E., & Beven, K. J. (2010). Flood-plain mapping: a critical discussion of deterministic and probabilistic approaches. *Hydrological Sciences Journal–Journal des Sciences Hydrologiques*, *55*(3), 364–376. https://doi.org/10.1080/02626661003683389

Dhondia, J. F., & Stelling, G. S. (2002). Application of one-dimensional two-dimensional integrated hydraulic model for flood simulation and damage assessment. Paper presented at 5th International Conference in Hydroinformatics, Cardiff, UK.

Doherty, J. E. (2010) *PEST, Model-Independent Parameter Estimation – User Manual. 5th ed., with slight additions.* Brisbane, Australia: Watermark Numerical.

Domeneghetti, A., Vorogushyn, S., Castellarin, A., Merz, B., & Brath, A. (2013). Probabilistic flood hazard mapping: effects of uncertain boundary conditions. *Hydrology and Earth System Sciences*, *17*(8), 3127–3140. https://doi.org/10.5194/hess-17-3127-2013

Dottori, F., Di Baldassarre, G., & Todini, E. (2013). Detailed data is welcome, but with a pinch of salt: accuracy, precision, and uncertainty in flood inundation modeling. *Water Resources Research*, *49*(9), 6079–6085. https://doi.org/10.1002/wrcr.20406

European Commission. (2007). *Directive 2007/60/EC of the European Parliament and of the Council of 23 October 2007 on the assessment and management of flood risks*. In Official Journal 6 November 2007 L 288/27. Brussels: European Commission.

FEMA (2016). *Guidance for Flood Risk Analysis and Mapping*. U.S. Department of Homeland Security.

FLOODsite (2007). *Failure Mechanisms for Flood Defence Structures*. Report Number T04-06-01. www.floodsite.net

FLOODsite (2009). *FLOODsite Final Report – Volume 1, Advancement in knowledge and understanding*. Report Number T35-09-01. www.floodsite.net

Gouldby, B., Sayers, P., Mulet-Marti, J., Hassan, M. A. A. M., & Benwell, D. (2008). A methodology for regional-scale flood risk assessment. *Proceedings of the Institution of Civil Engineers - Water Management*, *161*(3), 169–182. https://doi.org/10.1680/wama.2008.161.3.169

Hall, J. W., Dawson, R. J., Sayers, P. B., Rosu, C., Chatterton, J. B., & Deakin, R. (2003). A methodology for national-scale flood risk assessment. *Proceedings of the Institution of Civil Engineers-Water Maritime and Engineering*, *156*(3), 235–248. https://doi.org/10.1680/wame.2003.156.3.235

Hall, J., & Solomatine, D. (2008). A framework for uncertainty analysis in flood risk management decisions. *International Journal of River Basin Management*, *6*(2), 85–98. https://doi.org/10.1080/15715124.2008.9635339

Harvey, H., Hall, J., & Manning, L. (2014). Computing flood risk in locations protected by flood defences. *Proceedings of the Institution of Civil Engineers - Water Management*, *167*(1), 38–50. https://doi.org/10.1680/wama.12.00106

Henderson, D., & Plaschko, P. (2006). Stochastic Variables and Stochastic Processes. In *Stochastic Differential Equations in Science and Engineering* (pp. 1–54). Singapore: World Scientific Publishing. https://doi.org/10.1142/9789812774798_0001

Hesselink, A. W., Stelling, G. S., Kwadijk, J. C. J., & Middelkoop, H. (2003). Inundation of a Dutch river polder, sensitivity analysis of a physically based inundation model using historic data. *Water Resources Research*, *39*(9), 1234–1250. https://doi.org/10.1029/2002WR001334

Horritt, M. S., & Bates, P. D. (2002). Evaluation of 1D and 2D numerical models for predicting river flood inundation. *Journal of Hydrology*, *268*(1–4), 87–99. https://doi.org/10.1016/S0022-1694(02)00121-X

Horritt, M. S., Di Baldassarre, G., Bates, P. D., & Brath, A. (2007). Comparing the performance of a 2-D finite element and a 2-D finite volume model of floodplain inundation using airborne SAR imagery. *Hydrological Processes*, *21*(20), 2745–2759. https://doi.org/10.1002/hyp.6486

Horritt, M. S., Bates, P. D., Fewtrell, T. J., Mason, D. C., & Wilson, M. D. (2010). Modelling the hydraulics of the Carlisle 2005 flood event. *Proceedings of the Institution of Civil Engineers - Water Management*, *163*(6), 273–281. https://doi.org/10.1680/wama.2010.163.6.273

IMPACT (2005). *Final Technical Report*. www.impact-project.net

Jung, Y., & Merwade, V. (2015). Estimation of uncertainty propagation in flood inundation mapping using a 1-D hydraulic model. *Hydrological Processes*, *29*(4), 624–640. https://doi.org/10.1002/hyp.10185

Kamrath, P., Disse, M., Hammer, M., & Köngeter, J. (2006). Assessment of discharge through a dike breach and simulation of flood wave propagation. *Natural Hazards*, *38*(1–2), 63–78. https://doi.org/10.1007/s11069-005-8600-x

Khilar, K. C., Fogler, H. S., & Gray, D. H. (1985). Model for piping-plugging in earthen structures. *Journal of Geotechnical Engineering*, *111*(7), 833–846. https://doi.org/10.1061/(ASCE)0733-9410(1985)111:7(833)

Lendering, K., Schweckendiek, T., & Kok, M. (2018). Quantifying the failure probability of a canal levee. *Georisk: Assessment and Management of Risk for Engineered Systems and Geohazards*, *12*(3), 203–217. https://doi.org/10.1080/17499518.2018.1426865

Liu, Q., Qin, Y., Zhang, Y., & Li, Z. (2015). A coupled 1D–2D hydrodynamic model for flood simulation in flood detention basin. *Natural Hazards*, *75*(2), 1303–1325. https://doi.org/10.1007/s11069-014-1373-3

Maione, U., Mignosa, P., & Tomirotti, M. (2003). Regional estimation of synthetic design hydrographs. *International Journal of River Basin Management*, *1*(2), 151–163. https://doi.org/10.1080/15715124.2003.9635202

Marijnissen, R., Kok, M., Kroeze, C., & van Loon-Steensma, J. (2019). Re-evaluating safety risks of multifunctional dikes with a probabilistic risk framework. *Natural Hazards and Earth System Sciences*, *19*(4), 737–756. https://doi.org/10.5194/nhess-19-737-2019

Martínez-Gomariz, E., Gómez, M., Russo, B., & Djordjević, S. (2018). Stability criteria for flooded vehicles: a state-of-the-art review. *Journal of Flood Risk Management*, *11*, S817–S826. https://doi.org/10.1111/jfr3.12262

Masoero, A., Claps, P., Asselman, N. E. M., Mosselman, E., & Di Baldassarre, G. (2013). Reconstruction and analysis of the Po River inundation of 1951. *Hydrological Processes*, *27*(9), 1341–1348. https://doi.org/10.1002/hyp.9558

Mazzoleni, M., Bacchi, B., Barontini, S., Di Baldassarre, G., Pilotti, M., & Ranzi, R. (2014). Flooding hazard mapping in floodplain areas affected by piping breaches in the Po River, Italy. *Journal of Hydrologic Engineering*, *19*(4), 717–731. https://doi.org/10.1061/(ASCE)HE.1943-5584.0000840

Mazzoleni, M., Barontini, S., Ranzi, R., & Brandimarte, L. (2015). Innovative probabilistic methodology for evaluating the reliability of discrete levee reaches owing to piping. *Journal of Hydrologic Engineering*, *20*(5), 04014067. https://doi.org/10.1061/(ASCE)HE.1943-5584.0001055

Mazzoleni, M., Dottori, F., Brandimarte, L., Tekle, S., & Martina, M. L. V. (2017). Effects of levee cover strength on flood mapping in the case of levee breach due to overtopping. *Hydrological Sciences Journal*, *62*(6), 892–910. https://doi.org/10.1080/02626667.2016.1246800

Merwade, V., Olivera, F., Arabi, M., & Edleman, S. (2008). Uncertainty in flood inundation mapping: current issues and future directions. *Journal of Hydrologic Engineering*, *13*(7), 608–620. https://doi.org/10.1061/(ASCE)1084-0699(2008)13:7(608)

Merz, B., & Thieken, A. H. (2009). Flood risk curves and uncertainty bounds. *Natural Hazards*, *51*(3), 437–458. https://doi.org/10.1007/s11069-009-9452-6

Merz, B., Aerts, J., Arnbjerg-Nielsen, K., Baldi, M., Becker, A., Bichet, A., Blöschl, G., Bouwer, L. M., Brauer, A., Cioffi, F. et al. (2014). Floods and climate: Emerging perspectives for flood risk assessment and management. *Natural Hazards and Earth System Science*, *14*, 1921–1942. https://doi.org/10.5194/nhess-14-1921-2014

Milanesi, L., Pilotti, M., & Bacchi, B. (2016). Using web-based observations to identify thresholds of a person's stability in a flow. *Water Resources Research*, *52*(10), 7793–7805. https://doi.org/10.1002/2016WR019182

Milanesi, L., Pilotti, M., Belleri, A., Marini, A., & Fuchs, S. (2018). Vulnerability to flash floods: a simplified structural model for masonry buildings. *Water Resources Research*, *54*(10), 7177–7197. https://doi.org/10.1029/2018WR022577

Orlandini, S., Moretti, G., & Albertson, J. D. (2015). Evidence of an emerging levee failure mechanism causing disastrous floods in Italy. *Water Resources Research*, *51*(10), 7995-8011. https://doi.org/10.1002/2015WR017426

Palladino, M. R., Barbetta, S., Camici, S., Claps, P., & Moramarco, T. (2019). Impact of animal burrows on earthen levee body vulnerability to seepage. *Journal of Flood Risk Management*, e12559. https://doi.org/10.1111/jfr3.12559

Pappenberger, F., Beven, K., Horritt, M. S., & Blazkova, S. (2005). Uncertainty in the calibration of effective roughness parameters in HEC-RAS using inundation and downstream level observations. *Journal of Hydrology*, 302(1–4), 46–69. https://doi.org/10.1016/j.jhydrol.2004.06.036

1097 Pappenberger, F., Matgen, P., Beven, K. J., Henry, J. B., & Pfister, L. (2006). Influence of
1098 uncertain boundary conditions and model structure on flood inundation predictions. *Advances*
1099 *in Water Resources*, *29*(10), 1430–1449. https://doi.org/10.1016/j.advwatres.2005.11.012

1100 Pilotti, M., Maranzoni, A., Tomirotti, M., & Valerio, G. (2011). 1923 Gleno dam break: case
1101 study and numerical modeling. *Journal of Hydraulic Engineering*, *137*(4), 480–492.
1102 https://doi.org/10.1061/(ASCE)HY.1943-7900.0000327

1103 Pilotti, M., Maranzoni, A., Milanesi, L., Tomirotti, M., & Valerio, G. (2014). Dam-break
1104 modeling in alpine valleys. *Journal of Mountain Science*, *11*(6), 1429–1441.
1105 https://doi.org/10.1007/s11629-014-3042-0

1106 Romanowicz, R., & Beven, K. (2003). Estimation of flood inundation probabilities as
1107 conditioned on event inundation maps. *Water Resources Research*, *39*(3), 1073.

1108 Quirogaa, V. M., Kurea, S., Udoa, K., & Manoa, A. (2016). Application of 2D numerical
1109 simulation for the analysis of the February 2014 Bolivian Amazonia flood: application of the
1110 new HEC-RAS version 5. *Ribagua*, *3*(1), 25–33. https://doi.org/10.1016/j.riba.2015.12.001

1111 Sanyal, J. (2017). Uncertainty in levee heights and its effect on the spatial pattern of flood
1112 hazard in a floodplain. *Hydrological Sciences Journal*, *62*(9), 1483–1498.
1113 https://doi.org/10.1080/02626667.2017.1334887

1114 Sayers, P. B., Hall, J. W., & Meadowcroft, I. C. (2002). Towards risk-based flood hazard
1115 management in the UK. *Proceedings of the Institution of Civil Engineers - Civil Engineering*,
1116 *150*(5), 36–42. https://doi.org/10.1680/cien.2002.150.5.36

1117 Sayers, P. B., Wallis, M. J., Simm, J. D., Baxter, G., & Andryszewski, T. (2010). *Towards*
1118 *the Next Generation of Risk-Based Asset Management Tools*. Flood Risk Science and
1119 Management, 313–335. https://doi.org/10.1002/9781444324846.ch15

1120 Schultz, M. T., Gouldby, B. P., Simm, J. D., & Wibowo, J. L. (2010). Beyond the factor of
1121 safety: Developing fragility curves to characterize system reliability (Report No. ERDC-SR-
1122 10-1). Geotechnical and Structures Laboratory. Washington: US Army Corps of Engineers.

1123 Smemoe, C. M., Nelson, E. J., Zundel, A. K., & Miller, A. W. (2007). Demonstrating
1124 floodplain uncertainty using flood probability maps. *JAWRA Journal of the American Water*
1125 *Resources Association*, *43*(2), 359–371. https://doi.org/10.1111/j.1752-1688.2007.00028.x

1126 Surminski, S., & Thieken, A. H. (2017). Promoting flood risk reduction: The role of
1127 insurance in Germany and England. *Earth's Future*, *5*(10), 979–1001.
1128 https://doi.org/10.1002/2017EF000587

1129 Tayefi, V., Lane, S. N., Hardy, R. J., & Yu, D. (2007). A comparison of one- and two-
1130 dimensional approaches to modelling flood inundation over complex upland floodplains.
1131 *Hydrological Processes*, *21*(23), 3190–3202. https://doi.org/10.1002/hyp.6523

1132 Teng, J., Jakeman, A. J., Vaze, J., Croke, B. F., Dutta, D., & Kim, S. (2017). Flood
1133 inundation modelling: A review of methods, recent advances and uncertainty analysis.
1134 *Environmental Modelling & Software*, *90*, 201–216.
1135 https://doi.org/10.1016/j.envsoft.2017.01.006

Tyagunov, S., Vorogushyn, S., Muñoz Jimenez, C., Parolai, S., & Fleming, K. (2018). Multi-hazard fragility analysis for fluvial dikes in earthquake- and flood-prone areas. *Natural Hazards and Earth System Sciences*, *18*(9), 2345–2354. https://doi.org/10.5194/nhess-18-2345-2018.

Turitto, O., Cirio, C. G., Nigrelli, G., Bossuto, P., & Viale, F. (2010). Vulnerability of main Po River levees in the last 200 years. *L'Acqua*, *6*, 17–34 (in Italian).

USACE (1997). *Hydrology & Hydraulics Workshop on Risk-Based Analysis for Flood Damage Reduction Studies*. US Army Corps of Engineers, Pacific Grove, California.

USACE (1999). *Risk-based analysis in geotechnical engineering for support of planning studies*. (Engineer Technical Letter 1110-2-556). Washington: US Army Corps of Engineers.

USACE (2017). *Planning Risk Assessment for Flood Risk Management Studies*. (Regulation no. 1105-2-101). Washington: US Army Corps of Engineers.

Vacondio, R., Dal Palù, A., & Mignosa, P. (2014). GPU-enhanced finite volume shallow water solver for fast flood simulations. *Environmental Modelling & Software*, *57*, 60–75. https://doi.org/10.1016/j.envsoft.2014.02.003

Vacondio, R., Aureli, F., Ferrari, A., Mignosa, P., & Dal Palù, A. (2016). Simulation of the January 2014 flood on the Secchia River using a fast and high-resolution 2D parallel shallow-water numerical scheme. *Natural Hazards*, *80*(1), 103–125. https://doi.org/10.1007/s11069-015-1959-4

Van Der Most, H., & Wehrung, M. (2005). Dealing with uncertainty in flood risk assessment of dike rings in the Netherlands. *Natural Hazards*, *36*(1–2), 191–206. https://doi.org/10.1007/s11069-004-4548-5

Viero, D. P., D'Alpaos, A., Carniello, L., & Defina, A. (2013). Mathematical modeling of flooding due to river bank failure. *Advances in Water Resources*, *59*, 82–94.

Vorogushyn, S., Merz, B., & Apel, H. (2009). Development of dike fragility curves for piping and micro-instability breach mechanisms. *Natural Hazards and Earth System Sciences*, *9*(4), 1383–1401. https://doi.org/10.5194/nhess-9-1383-2009

Vorogushyn, S., Merz, B., Lindenschmidt, K. E., & Apel, H. (2010). A new methodology for flood hazard assessment considering dike breaches. *Water Resources Research*, *46*(8), W08541. https://doi.org/10.1029/2009WR008475

Vorogushyn, S., Apel, H., & Merz, B. (2011). The impact of the uncertainty of dike breach development time on flood hazard. *Physics and Chemistry of the Earth, Parts A/B/C*, *36*(7–8), 319–323. https://doi.org/10.1016/j.pce.2011.01.005

Wagenaar, D. J., De Bruijn, K. M., Bouwer, L. M., & Moel, H. D. (2016). Uncertainty in flood damage estimates and its potential effect on investment decisions. *Natural Hazards and Earth System Sciences*, *16*(1), 1–14. https://doi.org/10.5194/nhess-16-1-2016

Wahl, T. L. (2004). Uncertainty of predictions of embankment dam breach parameters. *Journal of Hydraulic Engineering*, *130*(5), 389–397. https://doi.org/10.1061/(ASCE)0733-9429(2004)130:5(389)

1175 Winter, B., Schneeberger, K., Huttenlau, M., & Stötter, J. (2018). Sources of uncertainty in a
1176 probabilistic flood risk model. *Natural Hazards*, *91*(2), 431–446.
1177 https://doi.org/10.1007/s11069-017-3135-5

1178 Wolff, T. F. (1997). *Geotechnical reliability of levees*. Paper presented at the USACE
1179 Hydrology and Hydraulics Workshop on Risk-Based Analysis for Flood Damage Reduction
1180 Studies, Pacific Grove, California.

List of figure captions

Figure 1. Diagram of the method for probabilistic flood hazard mapping. The light blue and green boxes indicate model inputs and outputs, respectively, while the grey boxes represent the modules of the method.

Figure 2. Sketch of levee geometries for piping failure analysis: (a) landside levee toe higher than the riverside floodplain; (b) landside levee toe lower than the riverside floodplain.

Figure 3. Example of fragility curve for piping at a levee section (left-hand side) and sensitivity on the modal value n_0 of the porosity in the range (n_{min}, n_{max}) (right-hand side). *WL* denotes the water level at the riverside levee bank above a reference horizontal datum (e.g., the sea level).

Figure 4. Sketch for the application of the probability multiplication rule to assess the probability of different levee breach scenarios. Labels LS_i (i = 1, …, N) refer to the "pre-selected" levee sections; label k (= 1, …, N_i) refers to different hydraulic loadings; *WL* denotes the water level.

Figure 5. Flood hazard classification by DEFRA (2006) for people.

Figure 6. Reach of the Po River (northern Italy) between the gauging stations of Cremona (upstream) and Borgoforte (downstream), levee system and cross sections. Plan view of the study area and 2D computational domain.

Figure 7. Boundary conditions used in the simulations: (a) inflow hydrograph of 100-year return period at the Cremona gauging station; (b) rating curve at the downstream section (Borgoforte gauging station).

Figure 8. Probabilistic levee breach map for the 100-year return period flood event. The probabilities reported are the sum of the probabilities of all the breach scenarios concerning the same levee section.

Figure 9. Probabilistic inundation extent map for the 100-year return period flood event.

Figure 10. Probabilistic maximum inundation depth maps for the 100-year return period flood event: (a) 75th, (b) 90th, (c) 99th percentile, and (d) probability-weighted average values.

Figure 11. Probabilistic maps for four hazard levels according to the DEFRA classification: (a) low; (b) moderate; (c) significant; (d) extreme. The maps refer to the 100-year return period flood event.

Figure 12. Probabilistic maximum hazard index maps for the 100-year return period flood event: (a) 75th, (b) 90th, (c) 99th percentile, and (d) probability-weighted average values.

Figure 1.

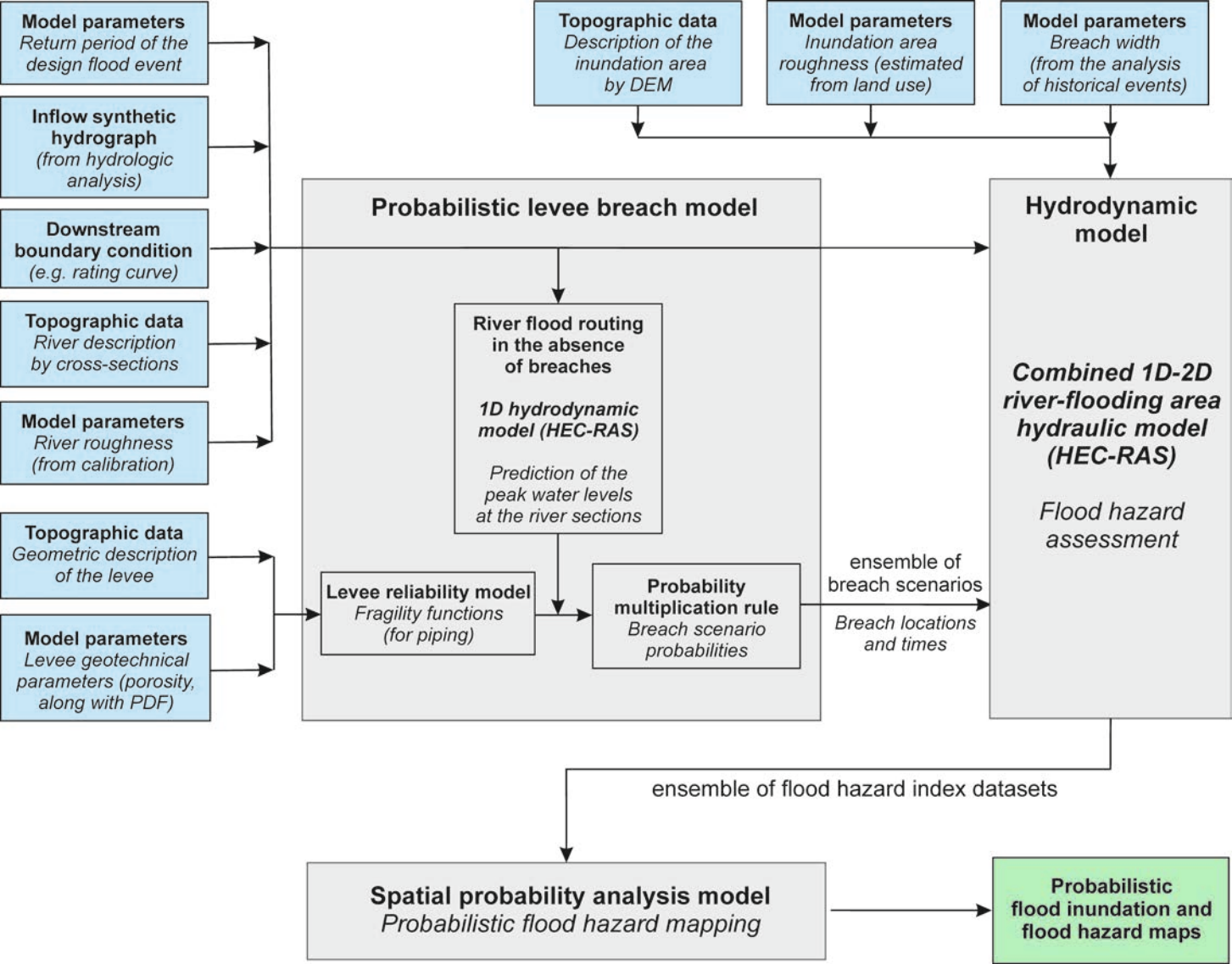
Model parameters
Return period of the design flood event
Inflow synthetic hydrograph
(from hydrologic analysis)
Downstream boundary condition
(e.g. rating curve)
Topographic data
River description by cross-sections
Model parameters
River roughness
(from calibration)
Topographic data
Geometric description of the levee
Model parameters
Levee geotechnical parameters (porosity, along with PDF)
Topographic data
Description of the inundation area by DEM
Model parameters
Inundation area roughness (estimated from land use)
Model parameters
Breach width
(from the analysis of historical events)
Probabilistic levee breach model
River flood routing in the absence of breaches
1D hydrodynamic model (HEC-RAS)
Prediction of the peak water levels at the river sections
Levee reliability model
Fragility functions
(for piping)
Probability multiplication rule
Breach scenario probabilities
ensemble of breach scenarios
Breach locations and times
Hydrodynamic model
Combined 1D-2D river-flooding area hydraulic model (HEC-RAS)
Flood hazard assessment
ensemble of flood hazard index datasets
Spatial probability analysis model
Probabilistic flood hazard mapping
Probabilistic flood inundation and flood hazard maps

Figure 2.

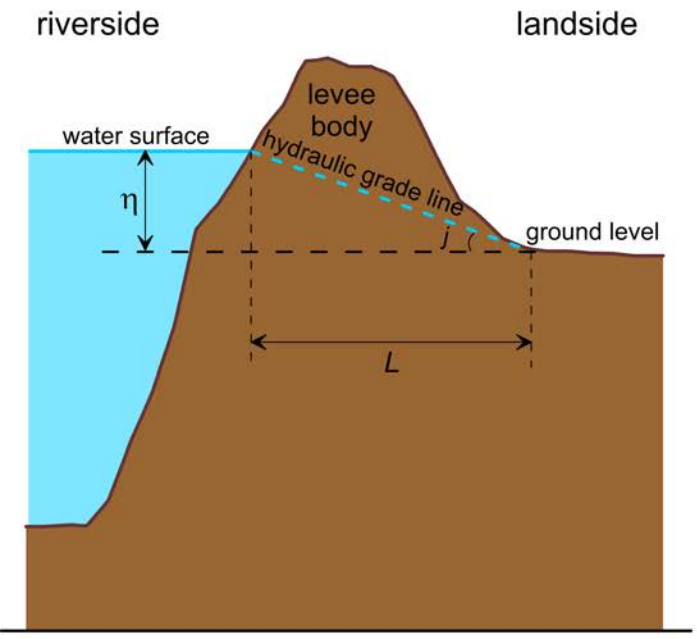
riverside
landside
levee
body
water surface
hydraulic grade line
η
j
ground level
L

(a)

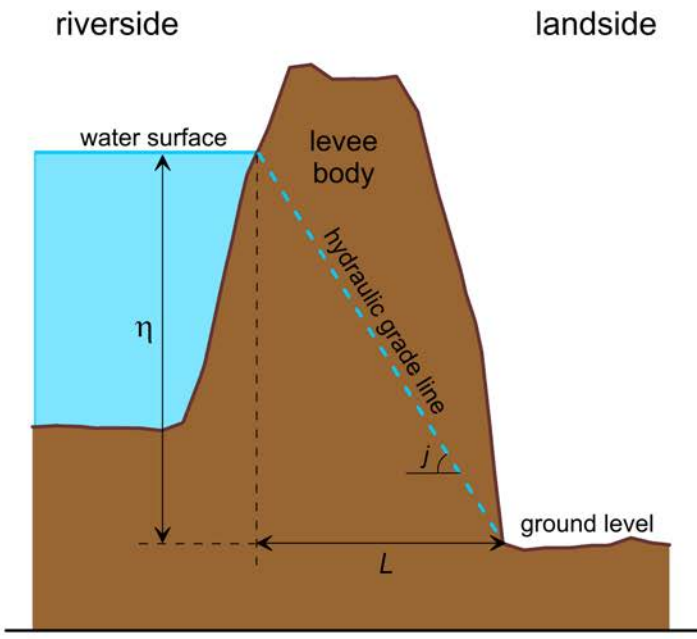
riverside
landside
water surface
levee
body
η
hydraulic grade line
j
ground level
L

(b)

Figure 3.

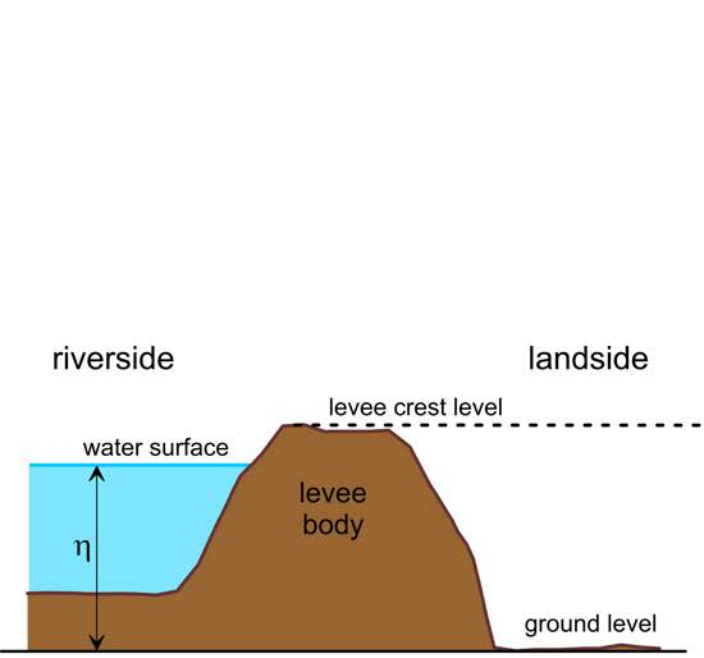
riverside
landside
levee crest level
water surface
levee body
η
ground level

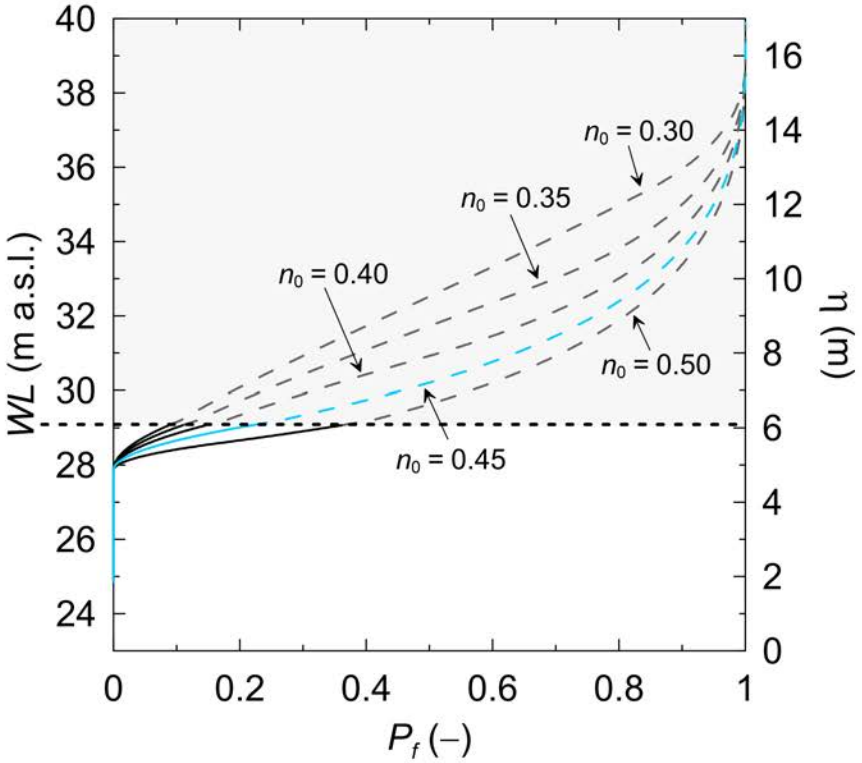
WL (m a.s.l.)
η (m)
P_f (–)
n_0 = 0.30
n_0 = 0.35
n_0 = 0.40
n_0 = 0.45
n_0 = 0.50
40
38
36
34
32
30
28
26
24
16
14
12
10
8
6
4
2
0
0
0.2
0.4
0.6
0.8
1

Figure 4.

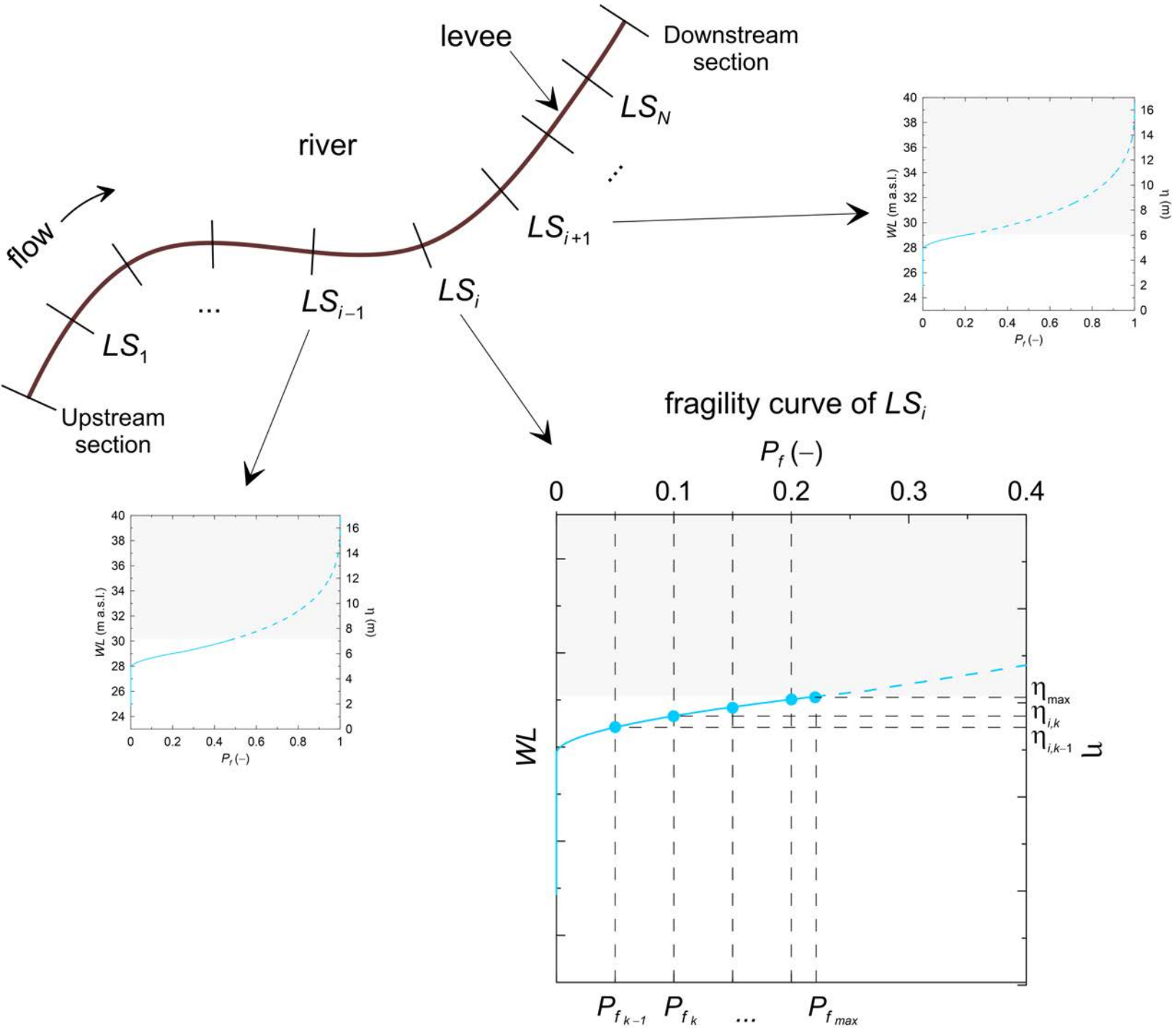
levee
Downstream section
LS_N
river
flow
LS_{i+1}
...
LS_{i-1}
LS_i
LS_1
Upstream section
WL (m a.s.l.)
η (m)
P_f (–)
fragility curve of LS_i
P_f (–)
0
0.1
0.2
0.3
0.4
WL
η
η_{max}
$\eta_{i,k}$
$\eta_{i,k-1}$
$P_{f\,k-1}$
$P_{f\,k}$
...
$P_{f\,max}$

Figure 5.

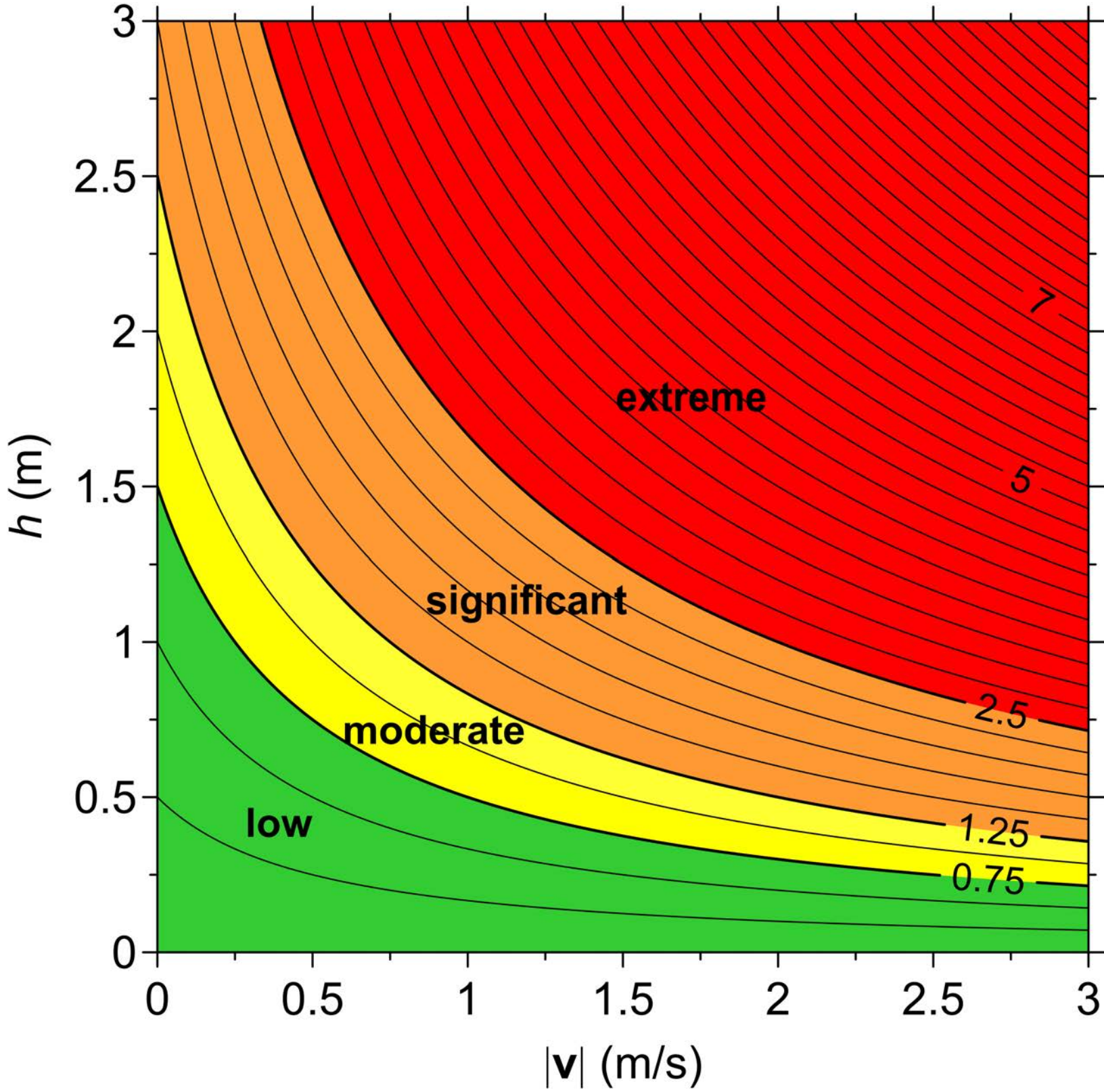
3
2.5
2
1.5
1
0.5
0
h (m)
0
0.5
1
1.5
2
2.5
3
|v| (m/s)
extreme
significant
moderate
low
7
5
2.5
1.25
0.75

Figure 6.

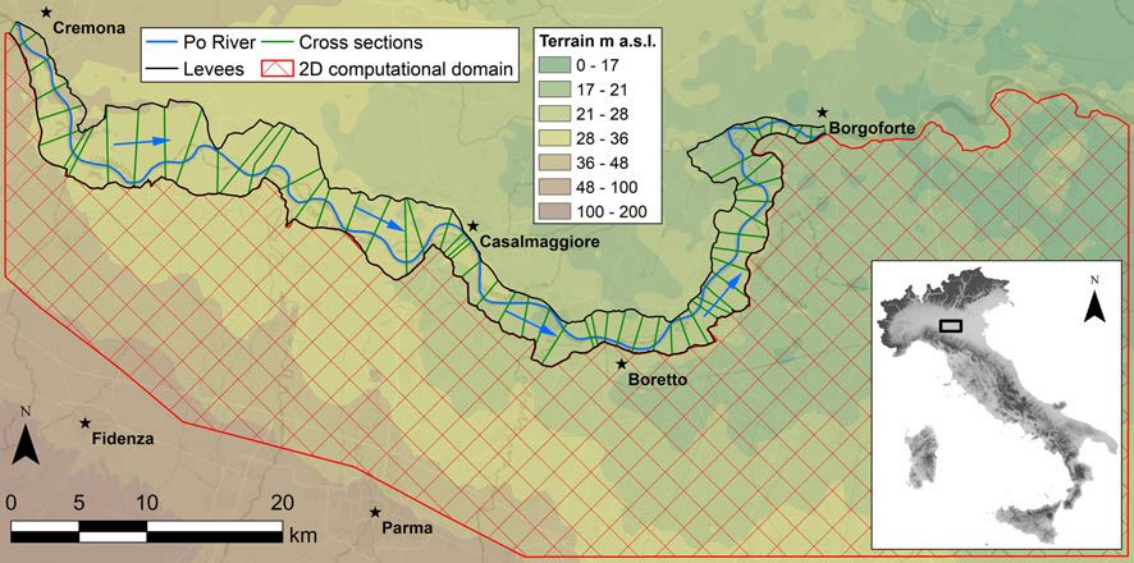
Cremona
Po River
Cross sections
Levees
2D computational domain
Terrain m a.s.l.
0 - 17
17 - 21
21 - 28
28 - 36
36 - 48
48 - 100
100 - 200
Borgoforte
Casalmaggiore
Boretto
N
Fidenza
0
5
10
20
km
Parma
N

Figure 7.

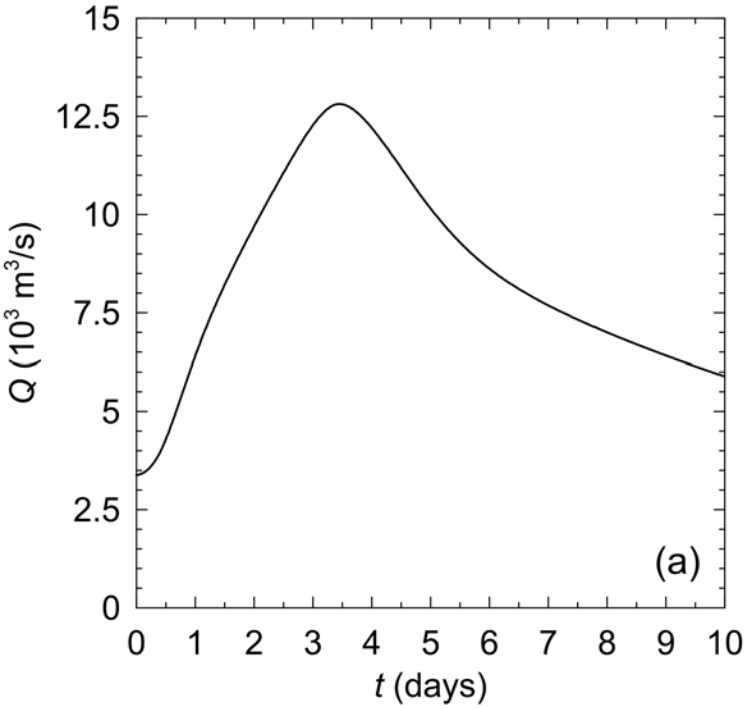
15
12.5
10
7.5
5
2.5
0
Q (10^3 m^3/s)
0 1 2 3 4 5 6 7 8 9 10
t (days)
(a)

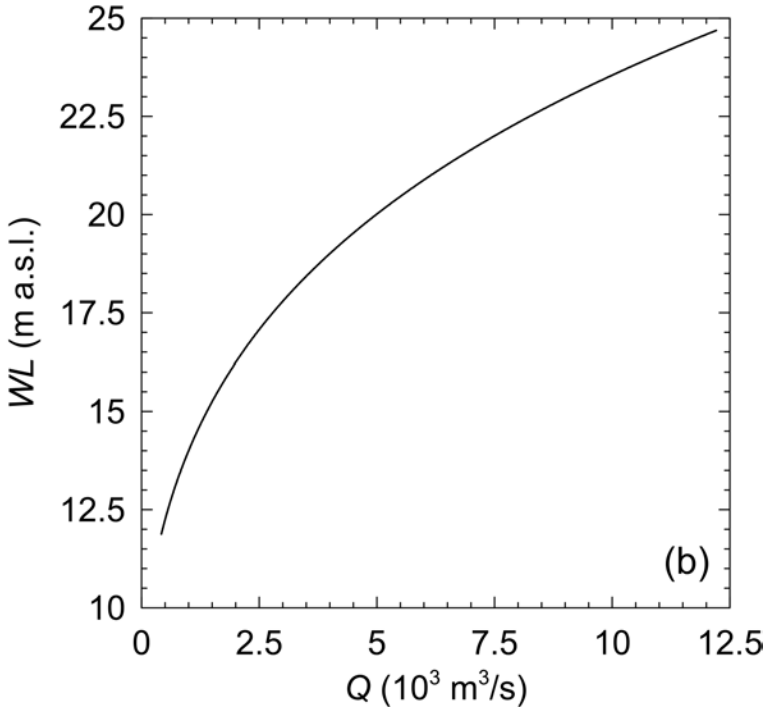
25
22.5
20
17.5
15
12.5
10
WL (m a.s.l.)
0 2.5 5 7.5 10 12.5
Q (10^3 m^3/s)
(b)

Figure 8.

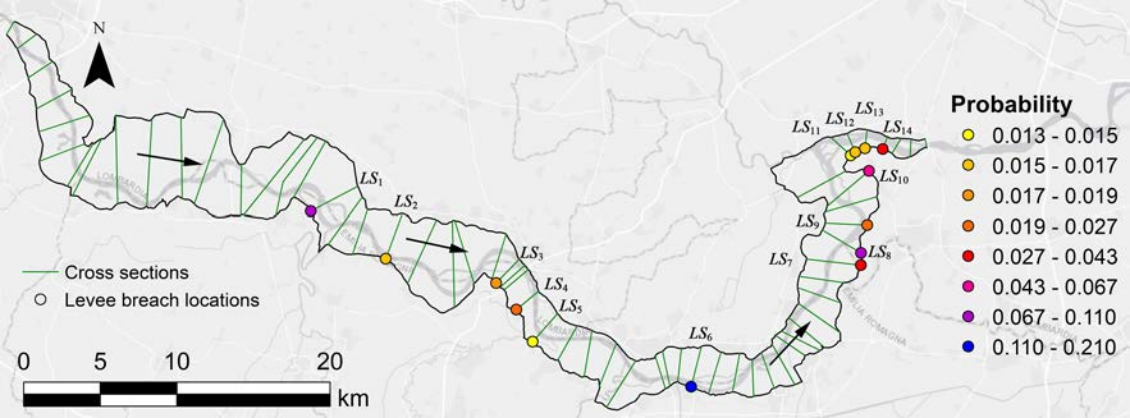
N
LS_1
LS_2
LS_3
LS_4
LS_5
LS_6
LS_7
LS_8
LS_9
LS_{10}
LS_{11}
LS_{12}
LS_{13}
LS_{14}
Cross sections
Levee breach locations
0
5
10
20
km
Probability
0.013 - 0.015
0.015 - 0.017
0.017 - 0.019
0.019 - 0.027
0.027 - 0.043
0.043 - 0.067
0.067 - 0.110
0.110 - 0.210

Figure 9.

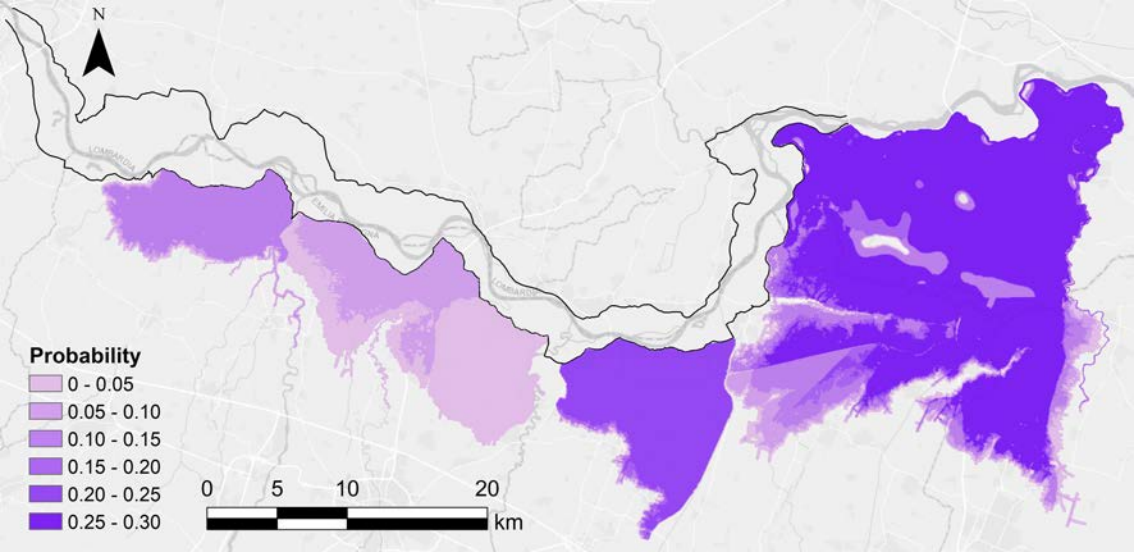
N
Probability
0 - 0.05
0.05 - 0.10
0.10 - 0.15
0.15 - 0.20
0.20 - 0.25
0.25 - 0.30
0
5
10
20
km

Figure 10.

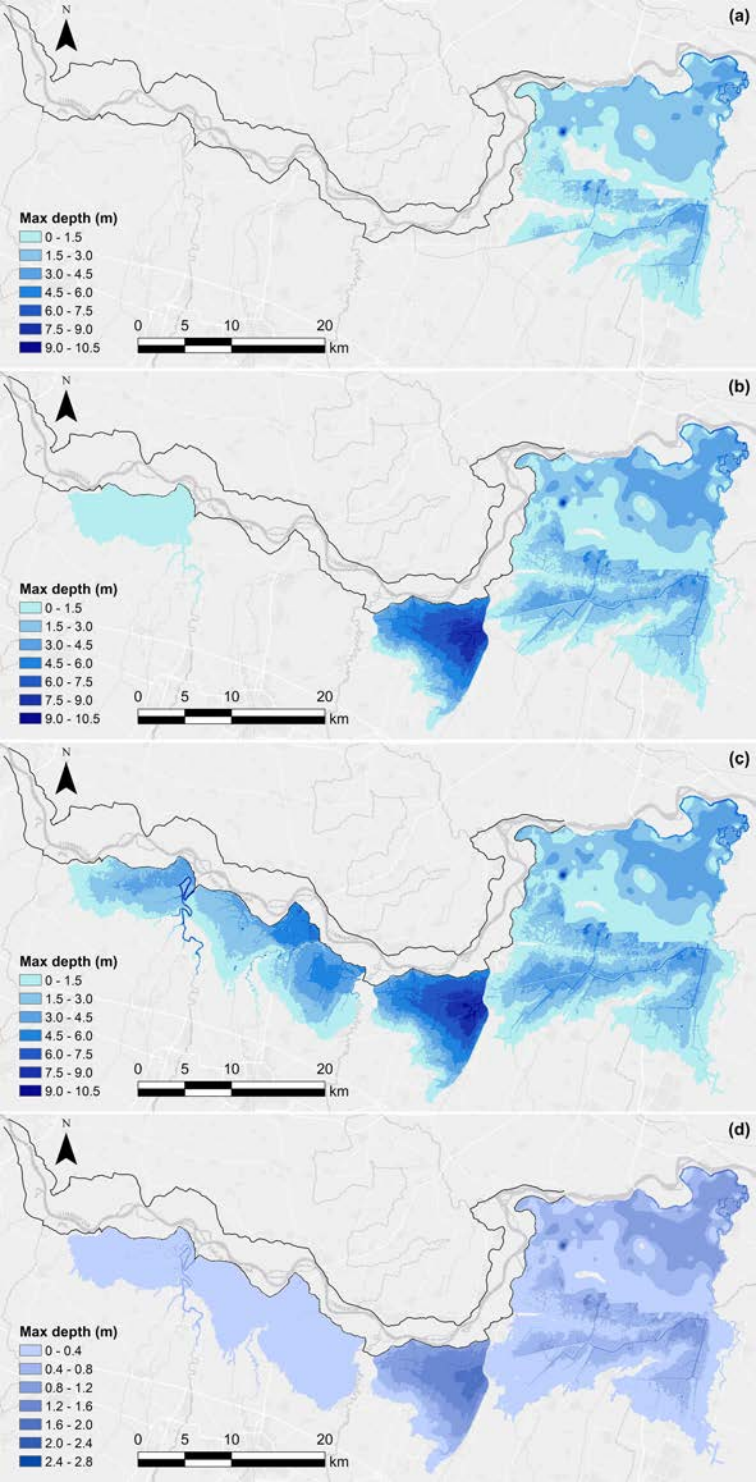
(a)
N
Max depth (m)
0 - 1.5
1.5 - 3.0
3.0 - 4.5
4.5 - 6.0
6.0 - 7.5
7.5 - 9.0
9.0 - 10.5
0 5 10 20
km
(b)
N
Max depth (m)
0 - 1.5
1.5 - 3.0
3.0 - 4.5
4.5 - 6.0
6.0 - 7.5
7.5 - 9.0
9.0 - 10.5
0 5 10 20
km
(c)
N
Max depth (m)
0 - 1.5
1.5 - 3.0
3.0 - 4.5
4.5 - 6.0
6.0 - 7.5
7.5 - 9.0
9.0 - 10.5
0 5 10 20
km
(d)
N
Max depth (m)
0 - 0.4
0.4 - 0.8
0.8 - 1.2
1.2 - 1.6
1.6 - 2.0
2.0 - 2.4
2.4 - 2.8
0 5 10 20
km

Figure 11.

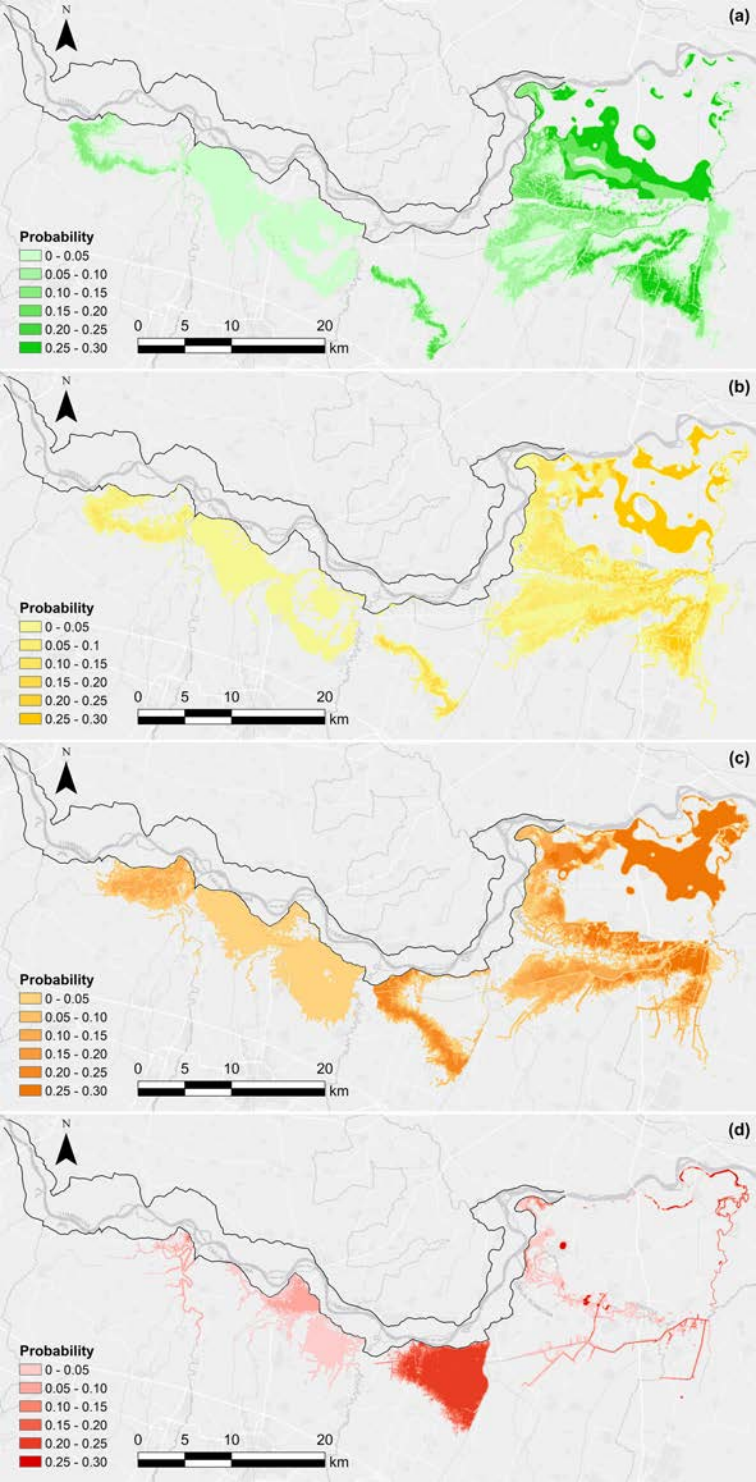
(a)
N
Probability
0 - 0.05
0.05 - 0.10
0.10 - 0.15
0.15 - 0.20
0.20 - 0.25
0.25 - 0.30
0 5 10 20
km
(b)
N
Probability
0 - 0.05
0.05 - 0.1
0.10 - 0.15
0.15 - 0.20
0.20 - 0.25
0.25 - 0.30
0 5 10 20
km
(c)
N
Probability
0 - 0.05
0.05 - 0.10
0.10 - 0.15
0.15 - 0.20
0.20 - 0.25
0.25 - 0.30
0 5 10 20
km
(d)
N
Probability
0 - 0.05
0.05 - 0.10
0.10 - 0.15
0.15 - 0.20
0.20 - 0.25
0.25 - 0.30
0 5 10 20
km

Figure 12.

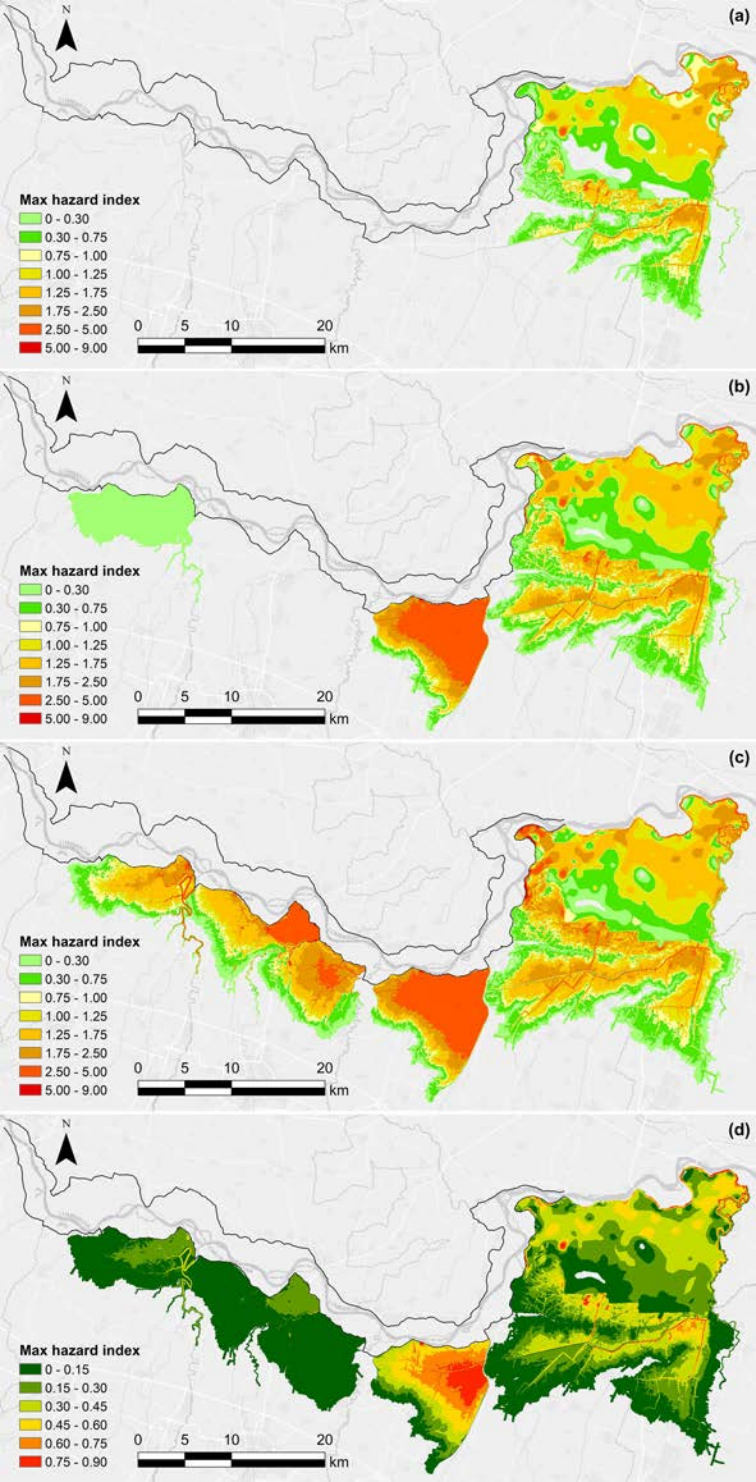
(a)
N
Max hazard index
0 - 0.30
0.30 - 0.75
0.75 - 1.00
1.00 - 1.25
1.25 - 1.75
1.75 - 2.50
2.50 - 5.00
5.00 - 9.00
0 5 10 20
km
(b)
N
Max hazard index
0 - 0.30
0.30 - 0.75
0.75 - 1.00
1.00 - 1.25
1.25 - 1.75
1.75 - 2.50
2.50 - 5.00
5.00 - 9.00
0 5 10 20
km
(c)
N
Max hazard index
0 - 0.30
0.30 - 0.75
0.75 - 1.00
1.00 - 1.25
1.25 - 1.75
1.75 - 2.50
2.50 - 5.00
5.00 - 9.00
0 5 10 20
km
(d)
N
Max hazard index
0 - 0.15
0.15 - 0.30
0.30 - 0.45
0.45 - 0.60
0.60 - 0.75
0.75 - 0.90
0 5 10 20
km